CHAPTER 2

Self-assembly of mesogens-decorated gold nanoparticles

2.1 Background & objectives

Although gold is the subject of one of the most ancient themes of investigation in science, its renaissance now leads to an explosive development in the fields of nanostructured materials, especially in the context of emerging nanoscience and nanotechnology with nanoparticles and self-assembled monolayers (SAMs). Gold nanoparticles are the most stable metal nanoparticles, and they present fascinating aspects such as, their self-assembly, the behaviour of individual particles, size related electronic, magnetic and optical properties, and their applications as catalysis [1] and in the bottom-up approach of nanotechnology. They also find applications in biological sciences [2, 3]. The synthesis of monolayer-protected gold nanoparticles (GNPs) in organic solvents by Brust and co-workers [4] has opened up a whole new field in materials science. The Brust method followed by several recent advances has allowed the facile synthesis of stable GNPs passivated with a variety of chemical functionalities [5-7]. These nanoparticles can be handled as simple organic materials and a variety of chemical reactions can be performed on functionalized GNPs [5-7]. These organic-stabilized metal nanoparticles have potential applications in the fields of catalysis, nonlinear optics, chemical and biological sensors, molecular recognition, nanotechnology, etc. [5-7].

On the other hand, as described in chapter 1, liquid crystals are attractive materials, since they show unique properties, such as long range order, cooperative effects and an anisotropic nature in optical and electronic properties based on the self-organizing nature in a certain temperature range with fluidity. Furthermore, their phase structures and molecular orientations

can be controlled easily and quickly by means of various external stimuli. These dynamic properties of liquid crystals enable us to apply liquid crystals not only to displays but also to various applications. Furthermore, by using the self-organizing nature of liquid crystals, highly ordered structures that are difficult to prepare by other methods are constructed [8].

Recently, metal nanoclusters, particularly gold nanoparticles, have attracted a great deal of interest since they show unusual properties compared to bulk metals. Since the properties of metal nanoclusters aggregates are affected by their morphology, various attempts to control their morphology have been performed by means of physical [9] and chemical processes [10]. What we need now, a control method, with reversible and simple process.

By providing metal nanoclusters with liquid crystalline properties, one could introduce the self-assembling ability and the reversible control of morphology of their aggregates by external stimuli, as well as the control of their properties by a simple and solvent free method. The reversible control of the properties of metal nanocluster aggregates will cultivate their potential as functional nanomaterials. The basic objective of this work is to incorporate GNPs into liquid crystalline systems. We approached the incorporation of GNPs into liquid crystalline systems by two ways.

By doping alkanethiol-protected GNPs into a discotic liquid crystalline matrix (section 2.2) and by attaching mesogens to GNPs (section 2.3 and 2.7). The most widely studied calamitic liquid crystal, alkoxycyanobiphenyl (section 2.3) and hexaalkoxytriphenylene as discotic liquid crystal (section 2.7) were selected to cover GNPs.

2.2 Inclusion of gold nanoparticles into a discotic liquid crystalline matrix

2.2.1 Synthesis

Well-known GNPs covered with hexanethiolate monolayer **1** (scheme 1) were prepared exactly following the reported method [11]. Thus, to a solution of tetraoctylammonium bromide (1.1 g) in toluene (65 ml) was added with stirring a solution of 158 mg of $HAuCl_4$. $3H_2O$. This solution was stirred for 20 minutes and mixed with n-hexanethiol (142 mg) with further stirring for 10 minutes. To this mixture, a solution of 450 mg of $NaBH_4$ dissolved in 5 ml of water was added. The reaction mixture was stirred at room temperature for 24 hours. The organic phase was separated, evaporated to about 2-3 ml in a rotary evaporator under vaccum at room temperature, mixed with 50 ml ethanol and centrifuged at 5000 rpm for 1 hour. The supernatant liquid was removed. The resulting hexanethiol-protected gold nanoparticles were dissolved in about 1 ml of dichloromethane and precipitated with ethanol. The centrifugation and redispersal process was repeated several times to ensure the complete removal of non-covalently bound organic material. Removal of the solvent afforded 60 mg of hexanethiol-capped gold nanoparticles.

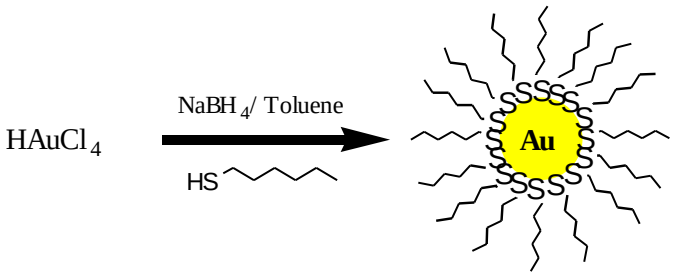

1

Scheme 1. Preparation of hexanethiol-covered gold nanoparticles.

It has been reported that this procedure furnished 1.6 nm core diameter nanoparticles with an average composition of $Au_{140}[S(CH_2)_5CH_3]_{53}$ [11]. The TEM image of hexanethiolate protected nanoparticles (figure 1) show majority of GNPs in the range of 1.4-2 nm.

2.2.2 Preparation & characterization of nanocomposites with discotic liquid crystals

Three types of DLCs were synthesized to prepare GNP-DLC composites (structure 2, 3, 4). These are hexahexylthiotriphenylene (HHTT) **2** displaying a highly ordered helical phase at lower temperature in addition to a hexagonal columnar mesophase [12], hexahexyloxytriphenylene (H6T) **3** having ordered hexagonal columnar phase [13] and hexakis[4-(4-methylnonyl)phenylethynyl]benzene **4** showing a discotic nematic phase at room temperature [14]. Binary mixtures of GNPs with DLCs were prepared by mixing the two components in dichloromethane followed by removal of solvent and drying in vacuum. Four compositions (by weight) of GNPs: HHTT (**2a**, 1:4; **2b**, 1:3; **2c**, 1:2; **2d**, 1:1), five compositions of GNPs: H6T (**3a**; 1:3; **3b**; 1:2; **3c**; 1:1, **3d**; 2:1, **3e**; 3:1) and 1:1 mixture GNPs-**4** (**4a**) were prepared and analyzed by differential scanning calorimetry (DSC) and polarizing optical microscopy (POM).

All the GNP-triphenylene DLC composites were found to be liquid crystalline in nature. They show classical textures of columnar mesophase upon cooling from the isotropic phase (figure 2). Data obtained from the heating and cooling cycles of DSC for GNP-HHTT composites are collected in Table 1. The DSC traces obtained on heating and cooling runs for **2** (HHTT) and for **2a** (HHTT-GNPs; 2:1 mixture) are shown in figure 3 and figure 4, respectively.

As may be seen from the data, increasing the amount of GNPs decreases the mesophase isotropic temperature but the crystals to mesophase or mesophase to mesophase (helical phase to columnar phase) temperatures do not change significantly. Similarly, all the GNP-H6T composites were also found to be liquid crystalline. Data collected from the heating and cooling cycles of DSC for GNP-H6T composites **3a**, **3b**, **3c**, **3d** and **3e** are collected in table 2. The DSC

traces obtained on heating and cooling runs for **3c** (H6T-GNPs; 1:1 mixture) is shown in figure 5.

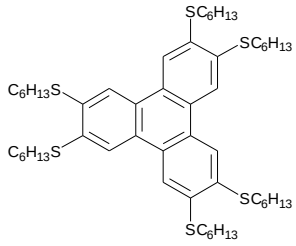

2

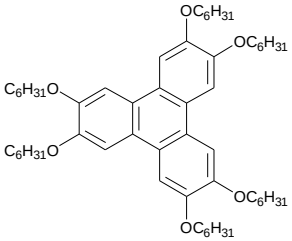

3

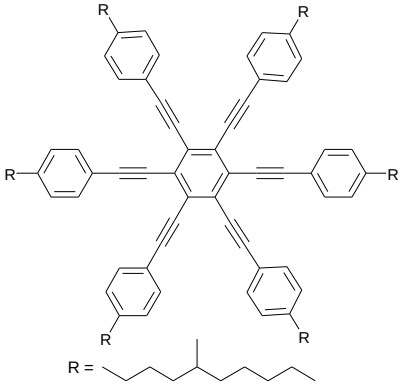

4

Chemical structures of (**2**) hexahexylthiotriphenylene, (**3**) hexahexyloxytriphenylene and (**4**) hexakis[4-(4-methylnonyl)phenylethynyl]benzene

Table 1. DSC results of GNPs-HHTT composites. Cr = crystal, H = helical phase, Col_h = hexagonal columnar mesophase, I = isotropic

Composite	Thermal transitions/°C	
	Heating scan	Cooling scan
2	Cr 67 H 74.9 Col_h 93.4 I	I 91.1 Col_h 66.8 H
2a	Cr 66.4 H 74.1 Col_h 90.1 I	I 86 Col_h 65.7 H
2b	Cr 67 H 74.7 Col_h 90.3 I	I 85.8 Col_h 65.8 H
2c	Cr 66.9 H 73.9 Col_h 88.3 I	I 83.6 Col_h 65.7 H
2d	Cr 67.7 H 74.4 Col_h 86.6 I	I 81.6 Col_h 65.5 H

Table 2. DSC results of GNP-H6T composites.

Composite	Thermal transitions/°C	
	Heating scan	Cooling scan
3	Cr 68.2 Col_h 99.4 I	I 97.9 Col_h 54.5 Cr
3a	Cr 67.3 Col_h 92.5 I	I 88.2 Col_h 49.0 Cr
3b	Cr 67.4 Col_h 94.6 I	I 90.3 Col_h 49.9 Cr
3c	Cr 67.7 Col_h 92.1 I	I 87.0 Col_h 49.3 Cr
3d	Cr 66.9 Col_h 84.5 I	I 78.5 Col_h 49.0 Cr
3e	Cr 66.6 Col_h 74.8 I	I 65.8 Col_h 47.1 Cr

In all the composites, the mesophase to the isotropic temperature broadened from about 2 °C to about 8 °C indicating a co-existence of the two phases. As may be seen from the DSC data plotted in figure 6, increasing the amount of GNPs decreases the mesophase isotropic temperature but the crystals to mesophase temperatures do not change significantly. This is logical as GNPs are expected to disturb core-core interaction and, therefore, disruption of cores i.e., mesophase to isotropic temperature would be most affected. Phase segregation is also visible upon increasing the amount of GNPs. While H6T and hexanethiol-protected nanoparticle composites show mesophase, a clear phase separation at about 75 °C was observed in the case of discotic nematic-GNP (1:1) composite. In the nematic phase, there is only an orientational order without any positional order of molecules and therefore, the molecular interactions are not sufficient to hold the gold nanoparticles. On the other hand, in the columnar phases, the π-π interactions between aromatic cores are strong, which are likely to be responsible for retaining the nanoparticles in the column.

To check whether the inclusion of GNPs in the matrix of discotic liquid crystals increases the conductivity of these composites, we have measured the DC conductivity of the HHTT and HHTT:GNPs (1:1) composite by a four-point probe. Measurement of conductivity was carried out using a standard DC voltage source (Aplab India), Picoammeter (Keithley 840) and a DMM (Keithley 2000). The samples were introduced into a glass capillary by heating to isotropic stage and the cooled to room temperature along with two gold coated copper wires at two ends which gets sealed during cooling. The resistance values are based on the measured current at different DC voltage in steps of 5 V up to 30 V. Current measurements were also carried at different temperatures from 30 ± 1 °C to 90 ± 1 °C using the same measurement set-up.

The inclusion of gold nanoparticles in the matrix of discotic liquid crystals increases the conductivity of these composites. The results indicate 250 times enhancement in the conductivity of HHTT upon doping with GNPs. We also found that upon increasing the temperature, a steady increase in the current was observed as shown in figure 7.

2.3 Alkoxycyanobiphenyl-covered gold nanoparticles

The discovery of alkyl- and alkoxy-cyanobiphenyls [15] was revolutionary in the field of liquid crystals. These cyanobiphenyls, prepared by Gray *et al*., were the first known low melting stable nematics. They have become constituents of liquid crystal mixtures used in display technology and their various physical properties have been extensively studied [16]. In order to attach these molecules to other molecules and to prepare dimers, oligomers and polymers, a number of terminally functionalized alkoxycyanobiphenyls have been synthesized. These include bromo-, hydroxyl-, amino-, carboxy-, epoxy-, and olifine-terminated cyanobiphenyls [17]. Many interesting monomeric, oligomeric and polymeric materials have been derived from these

functionalized cyanobiphenyls [18]. To our surprise, while a variety of functionalized cyanobiphenyls are known, terminally thiol functionalized cyanobiphenyls have not yet been reported in literature. The terminally thiol-functionalized cyanobiphenyls are required to prepare alkoxycyanobiphenyl-covered GNPs. Therefore, we first describe the synthesis and characterization of novel thiol-functionalized alkoxycyanobiphenyls (section 2.4). After that we present the formation of self-assembled monolayers (SAMs) of these materials on gold surface (section 2.5 and 2.6) followed by synthesis and characterization of alkoxycyanobiphenyl-covered gold nanoparticles (section 2.7).

2.4 Synthesis of terminally thiol-functionalized alkoxycyanobiphenyls

The synthesis of terminally thiol-functionalized alkoxycyanobiphenyls is out-lined in scheme 2 and the details are given in the experimental section. Commercially available 4'-hydroxy-4-biphenylcarbonitrile **5** was alkylated under classical reaction conditions with an excess of the appropriate α, ω-dibromoalkane to obtain the ω-brominated product **6** [19]. The bromo-terminated alkoxycyanobiphenyl **6** was converted to thioacetate **7** by reacting with thioacetic acid. Hydrolysis of the thioacetate furnished the desired thiol-terminated alkoxycyanobiphenyl **9**. Compound **9** can also be prepared by the hydrolysis of Bunte salt **8** which in turns can be prepared from ω-brominated product **6** by treatment with thiolsulfate ion. However, the yield was low and, therefore, the first thioacetate method was preferred.

2.4.1 Characterization

All the compounds were purified by repeated column chromatography followed by crystallization and characterized from their ^{1}H NMR, ^{13}C NMR, IR, UV spectra and elemental

analysis. All the members of the series give similar spectra. Spectral data and elemental analysis of all the compounds were in good agreement with their structures, indicating the high purity of all the materials.

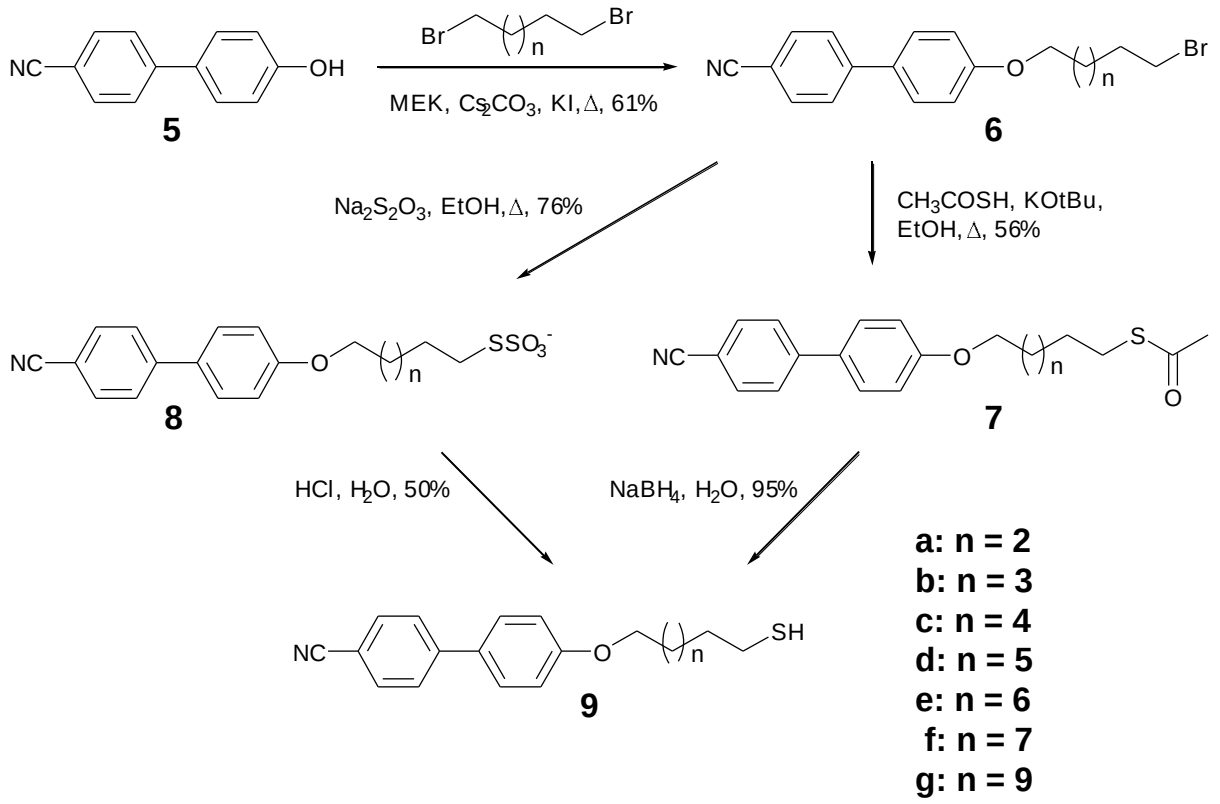

Scheme 2. Synthesis of terminally thiol-functionalized alkoxycyanobiphenyls.

Figure 8 shows the ^{1}H NMR spectrum of 4'-[(5-sulfanylpentyl)oxy][1,1'-biphenyl]-4-carbonitrile (**9a**). There are four different types of aromatic protons which give rise to four signals at different δ values.

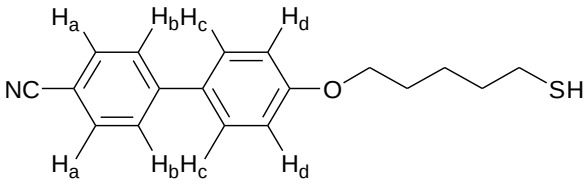

9a

As seen from the structure above, protons which are ortho to –CN group (H_a) are in the same environment and have the same δ values. These protons couple with the neighboring H_b protons and appear as doublet (d) and vice-versa. As they are (H_a, H_b) attached to aromatic ring having strongly electron withdrawing –CN group they have δ values higher compare to other hydrogens. Having ortho to –CN group H_a protons have highest δ values (δ = 7.7) in comparigion to H_b protons (δ = 7.6) and obviously, with respect to all other hydrogens. Similarly H_c and H_d protons appear as doublet with δ values 7.5 and 6.9 respectively. The $–SCH_2$ protons appear as a quartet at a δ value of 2.5 ppm. Other aliphatic protons of the chains can be clearly seen in the spectrum at δ 1.2-2.0 ppm. This confirms the structure and high purity of the compound. All other derivatives **9b-g** show similar spectrum differing only in the aliphatic protons and some of them are reproduced in figure 9 and figure 10.

Figure 11 is the reproduction of the ^{13}C NMR spectrum of compound **9b**. It gives only 8 carbon signals from the aromatic part (δ 160, 145, 132, 131, 128, 127, 116, 110), one signal from –CN (δ 119), one from $–O-CH_2$ (δ 68), one from $–S-CH_2$ (δ 39) and 4 signals (δ 31, 29, 28, 25) for methylene carbons. All other derivatives show similar ^{13}C NMR spectrum.

Elemental analyses of all the compounds give correct values with the errors +/- 0.4 %. All the elemental analysis data are in the experimental section.

Figure 12 shows the IR spectrum of the compound **9a**, which shows expected aromatic and aliphatic stretchings. A strong peak is observed for –CN group at 2200 cm^{-1}, and 2565 cm^{-1} for –SH group.

The UV spectra of all the samples were measured in CH_2Cl_2 and similar spectrum is obtained for all the compounds (**9a-g**). UV-Vis spectrum of the compound **9a** shows the absorption peaks at 330.8 nm.

2.4.2 Thermal behaviour

All the thiol-terminated alkoxycyanobiphenyls **9a-g** were found to be liquid crystalline with a very broad mesophase temperature range. The nature of these liquid crystals was studied by differential scanning calorimetry (DSC) and by optical microscopy with polarized light. Transition temperatures and transition enthalpies were determined by DSC. Data obtained from the heating and cooling cycles of DSC are collected in table 3 & 4. The peak temperatures are given in °C and the numbers in the parentheses indicate the transition enthalpy (ΔH) in KJ mol^{-1}. Table 3 presents the thermal behavior of precursor molecules **6** & **7** while the table 4 represents the thermal behavior of final compounds **9a-g**.

The lower homologues of the terminally bromo-substituted alkoxycyanobiphenyl series, display distinct monotropic nematic phase as seen from polarizing optical microscopy (POM) and differential scanning calorimetry (DSC). Compound **6a**, on heating, melts at about 82 ºC to the isotropic phase. On cooling N phase appears at 57 ºC which crystallizes at 46 ºC. Compound **6b**, on heating melts at 68 ºC to the isotropic phase and on cooling N phase appears at 62 ºC, which remains stable down to room temperature. Similarly, compound **6c** and **6e** exhibit monotropic nematic phase. On heating, they melt at about 65 ºC and 70 ºC to the isotropic phase. On cooling N phase appears at 59 ºC and 64 ºC, which crystallizes at 34 ºC and 62 ºC, respectively. Compound **6d**, **6f**, **6g** was found to be non-liquid crystalline. On heating, they show only one transition from crystal to isotropic phase. Compound **6d** on heating, melts at about 81 ºC to the isotropic phase and on cooling it crystallizes at about 70 ºC. Similarly, compound **6f** and **6g** show crystal to isotropic transition at about 77 ºC and 82 ºC, which crystallizes at 66 ºC and 68 ºC, respectively.

Table 3. Phase transition temperatures (peak, ºC) and associated enthalpy changes (KJ mol^{-1}, in parentheses) of terminally bromide & thioacetate-functionalized alkoxycyanobiphenyls. Cr: Crystalline phase; N: Nematic phase; I: Isotropic phase.

Compound	Heating scan	Cooling scan
6a	Cr 82.2 (29) I	I 57.1 (0.4) N 46.2 (26) Cr
6b	Cr 67.8 (31) I	I 61.5 (0.4) N
6c	Cr 65.4 (32) I	I 59.4 (0.6) N 34.2 (25) Cr
6d	Cr 81.0 (41) I	I 69.8 (41) Cr
6e	Cr 70.0 (48) I	I 64.2 (0.2) N 62 (29) Cr
6f	Cr 77.3 (50) I	I 65.6 (49) Cr
6g	Cr 82.6 (63) I	I 67.8 (30) Cr
7a	Cr 70.9 (27) I	I 52.4 (0.9) N 32.5 (15) Cr
7b	Cr 86.4 (41) I	I 49.8 (31) Cr
7c	Cr 84 (43) I	I 65 (43) Cr
7d	Cr 78.2 (45) I	I 51.4 (39) Cr
7e	Cr 74 (13) Cr 79 (46) I	I 62 (42) Cr
7f	Cr 71.3 (44) I	I 63.5 (44) Cr

Except compound **7a**, all the thio-acetate functionalized cyanobiphenyl series are found to be non-liquid crystalline. Compound **7a** on heating melts at about 71 ºC to the isotropic phase. On cooling, N phase appears at about 52 ºC which crystallizes at 32 ºC. Compound **7b**, **7c**, **7d**, **7f** on heating show a crystal to isotropic phase transition at 86 ºC, 84 ºC, 78 ºC, 71 ºC respectively.

On cooling they crystallize at 50 ºC, 65 ºC, 52 ºC, 64 ºC, respectively from the isotropic phase. Compound **7e** shows one crystal to crystal transition at 74 ºC before going to the isotropic phase at 79 ºC. On cooling it crystallizes at about 62 ºC.

Table 4. Phase transition temperatures (peak, ºC) and associated enthalpy changes (KJ mol^{-1}, in parentheses) of terminally thiol-functionalized alkoxycyanobiphenyls. Cr: Crystalline phase; N: Nematic phase; I: Isotropic phase.

Compound	Heating scan	Cooling scan
9a	Cr 54.9 (26) N 58.4 (0.3) I	I 57.2 (0.5) N
9b	Cr 56.0 (26) N 64.8 (0.2) I	I 63.5 (0.2) N
9c	Cr 60.1 (34) N 71.2 (0.5) I	I 70.4 (0.5) N 46.1 (33) Cr
9d	Cr 59.3 (39) N 64.8 (0.5) I	I 63.7 (0.4) N 39.8 (28) Cr
9e	Cr 67.8 (39) I	I 65.5 (0.7) N 49.4 (35) Cr
9f	Cr & N 67.3 (46) I	I 67.0 (0.7) N 56.2 (36) Cr
9g	Cr 67.6 (3) Cr 71.6 (16) I	I 61.7 (40) N and Cr

The lower homologues of the terminally thiol-substituted cyanobiphenyl series, **9a**, **9b**, **9c**, **9d**, display distinct Cr-N and N-I transition peaks in DSC. Compound **9a**, (4'-[(5-sulfanylpentyl)oxy][1,1'-biphenyl]-4-carbonitrile) shows enantiotropic nematic phase. On heating, it melts at about 54 °C to the nematic phase which clears at about 58 °C. On cooling, the nematic phase appears at about 57 °C (figure 13) and remains stable down to room temperature. Compound **9b** and **9c** exhibit an enantiotropic nematic phase. Upon heating, they melt at about

56 °C and 60 °C to the nematic phase which clears at about 65 °C and 70 °C, respectively. On cooling, the N phase appears with only about one degree of supercooling in both compounds. While the N phase of **9b** remains stable down to room temperature, the N phase of **9c** crystallizes at about 46 °C. The DSC and photomicrograph of **9c** is shown in figure 14 and 15 respectively. Compound **9d** also shows enantiotropic N phase. On heating it melts at about 59 °C to the N phase which clears at about 65 °C. On cooling, N phase appears at 64 °C which crystallizes at 49 °C. Compound **9e** shows a monotropic N phase. On heating, it shows only one transition from crystal to isotropic transition at 68 °C and on cooling N phase appears at 65.5 °C which crystallizes at 49 °C. Compound **9f**, on heating under POM, shows the co-existence of N and Cr phases between 64 and 68 °C before going to the isotropic phase. However, the first DSC heating run shows only a broad peak centered at 67.3 °C. On cooling the N phase appears at 67 °C with crystallization at 56 °C. Compound **9g** on slow heating (1 °C/min) shows a weak transition at 67.6 °C and another endothermic transition at 71.6 °C. On faster heating, these peaks do not resolve and only a broad endothermic transition is observed. On cooling the isotropic phase, a metastable nematic phase is discernable at 63 °C. The monotropic mesophase has a high crystallization tendency which starts in the mesophase and is completed at 61 °C. The first cooling DSC run shows only a broad transition centered at 61.7 °C.

2.4.3 X-ray diffraction studies

Diffraction pattern of the N phases of all the compounds show a diffuse peak in the wide angle region, in a direction normal to that of the magnetic field. It has a spacing of about 0.45 nm and corresponds to the average lateral separation of the molecules in these fluid phases. In the N phase of compound **9f** with the longer spacer a single sharp peak is observed in the small angle

region in the diffraction pattern along the field direction (figure 16). It has a spacing of 3.87 nm at 60 °C, which matches very well with the spacing expected from an antiparallel arrangment of two cyanobiphenyl moiety (figure 17). This peak shifts to 3.39 nm at 50 °C in the N phase of compound **9d**, consistent with the decrease in the length of the spacer. Similarly compound **9c** shows a sharp peak in the small angle region of the diffraction pattern with a spacing of about 3.12 nm in the N phase at 50 °C. Compounds **9b** and **9a** also show similar type of X-ray diffraction pattern with a spacing of about 2.91 and 2.49 nm in the small angle region. All spacings are roughly comparable to the antiparallel arrangment of two cyanobiphenyl moiety as described above.

2.4.4 Conclusion

As described already, only the nematic phase was observed in all the members of the terminally thiol-substituted cyanobiphenyl series. In contrast to the thermal behaviour of the much studied 4'-alkoxy-4-cyanobiphenyl series [20], no smectic phase is seen in the higher homologues of this series of derivatives. Similar results were reported earlier in the case of terminally hydroxy-, amino-, and carbioxylic acid-substituted alkoxycyanobiphenyls [17]. The non-appearance of the smectic phase in these terminally-functionalized alkoxycyanobiphenyls has been discussed previously [17h, 17m]. All the new thiol-teminated alkoxycyanobiphenyls form self-assembled monolayers on a gold surface (section 2.5). This is very useful to study the properties of these molecules in the nano scale.

2.5 Self-assembled monolayers (SAMs) of alkoxycyanobiphenyl thiols on gold: A study of electron transfer reaction using cyclic voltammetry and electrochemical impedance spectroscopy (In collaboration with Prof. V. Lakshminarayanan)

Self assembled monolayers, commonly known as SAMs, provide a convenient, flexible and simple system for studies in nanoscience and nanotechnology. It refers to a single layer of molecules adsorbed spontaneously by chemisorptions on the metallic surfaces such as Au, Ag, Pt, etc., to form highly ordered surfaces with fewer defects and exhibit a high degree of orientation, molecular ordering and packing density [21, 22]. Studies on film formation, structure and properties of SAM reported in literature are mostly based on aliphatic thiols [23]. Increasing attention in recent times on the monolayer-modified surfaces is due to their potential applications in a variety of fields such as photolithography [24], sensors [25], non-linear optical materials [26], microcontact printing [27], molecular wire and molecular electronics [28], high density memory storage devices [29] and corrosion protection [30]. Apart from these applications, the fundamental studies on interfacial electron transfer and electrochemical processes at the SAM-modified electrode/solution interface are also of interest and widely reported in literature [31]. The blocking ability of the monolayer-coated electrode to the electron transfer process is usually evaluated as redox probes [32]. Some ruthenium complexes in solutions have also been used a redox probes in many chemical, biological and photochemical sensors [33].

Apart from commonly studied SAMs of aliphatic thiols, there is also a great deal of interest on the monolayers of aromatic thiols [34] in recent times. SAMs of aromatic thiols are of interest owing to their higher rigidity and the presence of delocalized π-electrons in the aromatic ring. Among several aromatic thiols reported in literature, there are some scattered reports on SAM of biphenyl thiol [35]. Cyganik *et al*. reported the scanning tunneling microscopic

observation of the influence of spacer chain on the molecular packing of SAMs of ω-biphenylalkane thiols on Au (111) [35a]. Long *et al*. studied the effect of odd-even number of alkyl chains on SAMs of biphenyl-based thiols using cyclic voltammetry [35c].

A few reports on self-assembled monolayer of molecules, which show the liquid crystalline phase behaviour in bulk are also known. Both discotic and calamitic mesogens have been shown to form highly ordered SAMs on gold leading to many interesting properties and phenomena [36]. Terminally thiol functionalized mesogens are the precursor molecules for the preparation of these materials. Having terminally thiol-functionalised alkoxycyanobiphenyls in hand, we got the idea to look their self-assembling properties on gold.

Self-assembled monolayers (SAMs) of liquid crystalline thiol-terminated alkoxycyanobiphenyl molecules with different alkyl chain length on Au surface have been studied using cyclic voltammetry and electrochemical impedance spectroscopy (EIS) [37]. The barrier property of the SAM-modified surface was evaluated using two different redox probes, mainly potassium ferro/ferri cyanide and hexaammineruthenium (III) chloride.

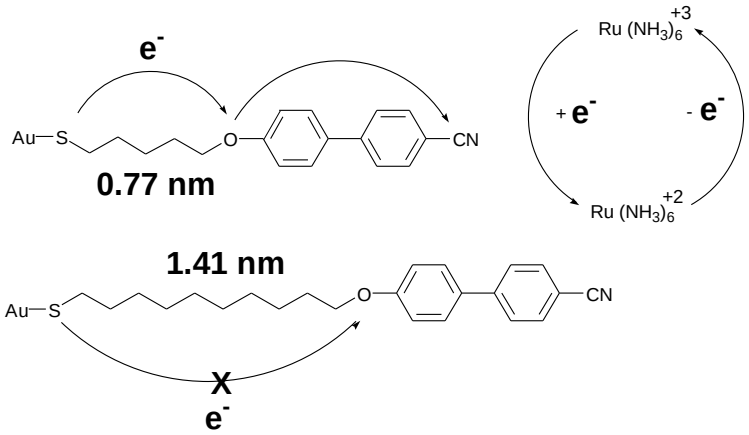

Scheme 3. The diagram of proposed mechanism for electron transfer reaction on SAM-modified electrodes using $[Ru(NH_3)_6]^{2+/3+}$ as redox probe.

It was found that for short length alkyl chain thiol (C5) the electron transfer reaction of hexaammineruthenum (III) chloride takes place through tunneling mechanism (scheme 3). In contrast, redox reaction of potassium ferro/ferri cyanide is almost completely blocked by the SAM-modified Au surface. From the impedance data, a surface coverage value of > 99.9 % was calculated for all the thiol molecules.

2.6 Self-assembled monolayers (SAMs) of alkoxycyanobiphenyl thiols on gold surface using a lyotropic liquid crystalline medium (In collaboration with Prof. V. Lakshminarayanan)

The self-assembled monolayers (SAMs) of alkoxycyanobiphenyl thiols on gold in a lyotropic liquid crystalline medium were studied using electrochemical technique [38]. Thiol-terminated alkoxycyanobiphenyls **9a**, **9d** and **9f** which exhibit nematic liquid crystalline order in bulk were used for this study. They are dispersed in a hexagonal lyotropic liquid crystalline phase, consisting of a non-ionic surfactant, Trition X-100 and water. This medium provides a highly hydrophobic environment to solubilize the thiols and later facilate their delivery to the gold surface to form a monolayer. The electrochemical technique such as, cyclic votammetry and electrochemical impedance spectroscopy were used to evaluate the barrier property and ionic permeability of these monolayers on gold surface. The results were compared with that of the corresponding monolayers prepared using dichloromethane as a solvent. It was observed that the monolayers prepared using hexagonal liquid crystalline phase show a better electrochemical blocking ability towards the redox reactions and exhibit very low ionic permeability. From the impedance data, a surface coverage of > 99.99% for the monolayer on Au surface for all the thiol molecules studied in this work was determined [38].

2.7 Synthesis and characterization of alkoxycyanobiphenyl covered GNPs

The liquid crystalline thiol ligand, 4'- (10-mercaptodecyloxy)biphenyl-4-carbontrile (**9f**), was synthesized from 4'-hydroxybiphenyl-4-carbonitrile via 3 steps (scheme 2) as described previously. Gold nanoparticles with LC ligands were synthesized according to the conventional two-phase protocol with $HAuCl_4$, tetraoctylammonium bromide (TOAB), and $NaBH_4$. Tetra-*n*-octylammonium bromide was used as a phase transfer reagent, and tetrachloroaurate (III) ion was reduced to Au (0) with sodium borohydride in the presence of mesogenic thiol (**9f**) in toluene (feed mole ratio, $AuCl_4^-$: **9f** = 1:3). The metal protected cluster (CNBP-GNP) was washed with ethanol and acetone several times and dried in vaccuo. It was obtained as a black powder, and could be redispersed easily in nonpolar solvents such as chlororoform, benzene, and hexane. The reduction of tetrachloroaurate (III) ion to Au (0) was confirmed by the appearance of a surface Plasmon absorption band at around 510 nm in a UV-Vis absorption spectrum measured in chloroform. The UV-Vis spectrum is reproduced in figure 18.

Figure 19 shows the ^1H NMR spectrum of fully covered alkoxycyanobiphenyl thiol-based gold nanoparticles in $CDCl_3$. In the ^1H NMR spectrum a proton signal around 2.5 ppm, which can be assigned to α-protons ($-CH_2SH$), disappeared and the broadening of all proton signals was observed. The disappearance of α-protons and the broadening of the proton signals demonstrates that all thiol molecules are covalently linked to the gold surface, *i.e.* there are no parent thiol molecules remained in the metal protected clusters. TLC supported this result. No spot corresponding to free thiol (**9f**) was observed on a TLC plate.

The CNBP-GNP was also characterized from its IR spectrum. It shows characteristic peak of –CN group at 2223 cm^{-1}. All other peaks are clearly visible in the spectrum. The IR spectrum is reproduced in figure 20.

Scanning tunneling microscopy imaging has been carried out in constant current mode using +100 mV sample bias voltage and 1 nA tunneling current to get the size of the individual nanoparticles. The mean diameter of CNBP-GNP's was determined to be *ca*. 3 nm by STM measurement. The image is shown in figure 21.

Our virgin CNBP-GNPs did not display any liquid crystalline behaviour. However, very recently, the same material was reported to be liquid crystalline by In *et al*. [39].

2.8 Discotic-decorated gold nanoparticles

2.8.1 Synthesis of thiol functionalized triphenylenes

To prepare triphenylene-covered gold nanoparticles, a triphenylene derivative having terminal thiol group was required. The monothiol-functionalized triphenylene derivative **16** was prepared as shown in scheme 4. Hexalkoxytriphenylene **12**, monohydroxytriphenylene **13** and ω-bromo-substituted triphenylene **14** were prepared following literature methods [40]. Thus oxidative trimerization of dialkoxybenzene **10** with $FeCl_3$ in presence of a catalytic amount of H_2SO_4 gives hexaalkoxytriphenylenes **11** in 65 % yield. Selective cleavage of one of the aryl-ether bond of **12** using B-bromocatecholborane furnished monohydroxytriphenylenes **13** in about 50 % yield. Monohydroxytriphenylene on reflux with appropriate dibromide in presence of Cs_2CO_3 as a base and ethyl methyl ketone as a solvent give rise to bromo-terminated triphenylene **14** in about 70 % yield. The bromo-terminated triphenylene **14** was converted to thioacetate **15** by reacting with thioacetic acid. Hydrolysis of the thioacetate furnished the desired 6-{[3,6,7,10,11-pentakis-(pentyloxy)-2-triphenylenyl]oxy}-1-pentanethiol **16**. The details of procedure are given in the experimental section.

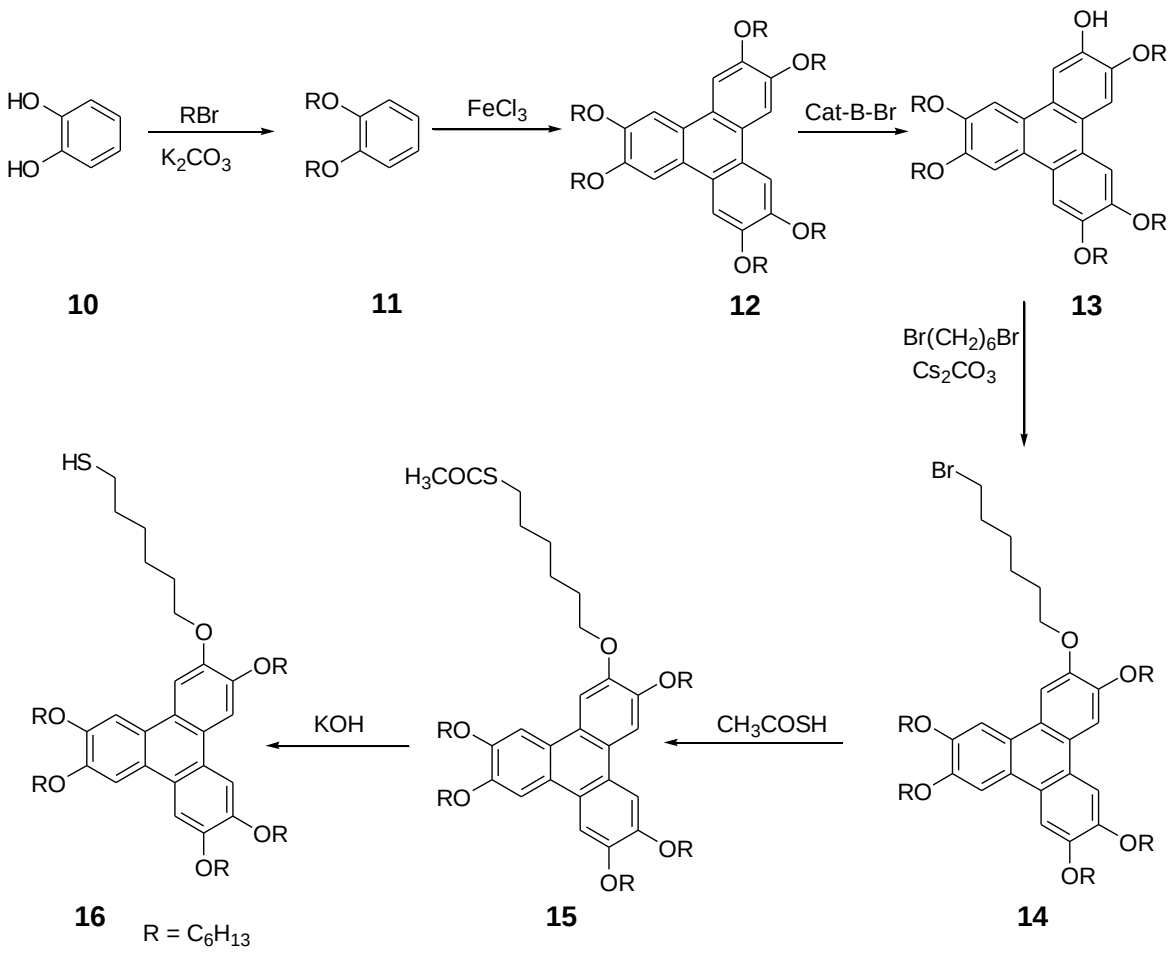

Scheme 4. Synthesis of thiol functionalized triphenylene.

2.8.2 Synthesis of triphenylene-decorated gold nanoparticles

Triphenylene-stabilized gold clusters **17** (scheme 5) were prepared by reducing $HAuCl_4$ with $NaBH_4$ in the presence of **16** closely following the method reported for the synthesis of alkanethiol-capped GNPs [11]. Thus, to a solution of tetraoctylammonium bromide (0.068 g), in toluene (5 ml) was added dropwise an aqueous solution of $HAuCl_4.3H_2O$ (11mg, 0.028 mmol) and the mixture was stirred for 20 minutes. The reaction mixture was washed with distilled water (10 ml) several times, and the organic layer was separated.

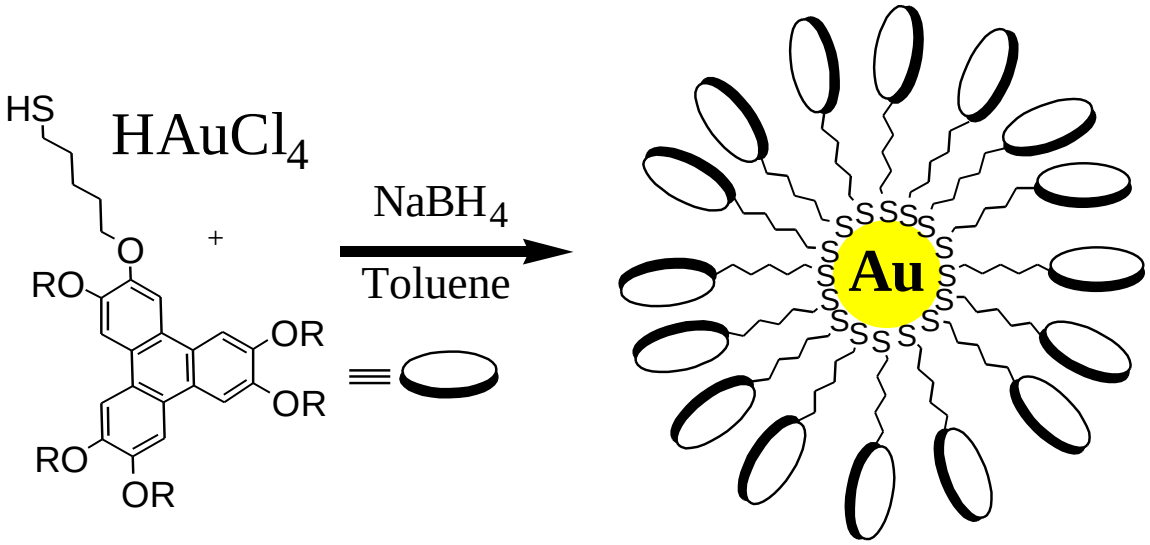

16 **17**

Scheme 5. Synthesis of gold nanoparticle covered with triphenylene ligands (**17**).

A solution of triphenylene thiol (33 mg, 0.038 mmol) in toluene (2 ml) was added to the above solution, and the resulting mixture was stirred for 30 minutes. An aqueous solution of $NaBH_4$ (11 mg, 0.28 mmol) was added dropwise, and the mixture was stirred for a further period of 3 hours. The organic layer was washed with distilled water and diluted with methanol (250 ml). It was kept in a refrigerator, and the precipitate obtained was further purified by being resuspended in toluene and centrifuged after the addition of methanol (10 ml). The centrifugation and re-dispersal process was repeated several times to ensure the complete removal of non-covalently bound organic material. These discotic functionalized gold nanoparticles were found to be highly soluble in common organic solvents like, dichloromethane, chloroform, THF, *etc*. ^{1}H NMR, UV and IR spectra (figure 22, 23 and 24 respectively) fully support the formation of triphenylene-covered gold nanoparticles.

Mixed monolayer covered GNPs (scheme 6, **18**) were prepared by mixing **1** (5 mg) and **17** (5 mg) in dichloromethane followed by removal of solvent in vacuum. The purification was performed as described above for hexanethiol-protected GNPs.

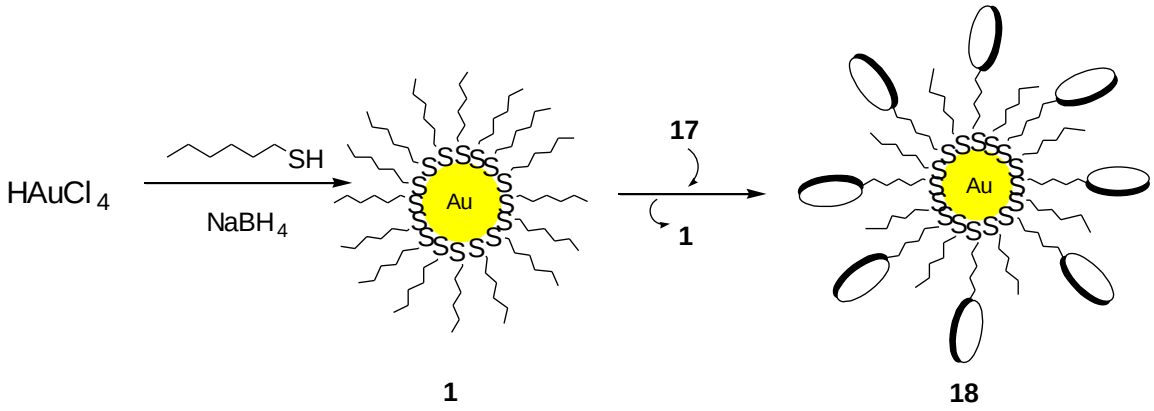

Scheme 6. Synthesis of mixed monolayer-covered gold nanoparticles.

2.8.3 Characterisation of triphenylene-covered gold nanoparticles

2.8.3.1 Transmission electron microscopy (TEM)

For the transmission electron microscope (TEM) measurement of these nanoparticles, one drop of the freshly prepared GNP-TP solution in CH_2Cl_2 (0.001g mL^{-1}) was placed on to the carbon supported copper grid, and dried at room temperature for two hours before the measurement. TEM images were recorded with a Hitachi H-7000 Electron Microscope, operating at 100 kV. Figure 25 shows typical TEM image of triphenylene-covered GNPs. The formation of spherical GNPs having an average size of about 2.4 nm was observed. The majority of the particles were of 2.4 nm sizes and only a few were in the range of 1.6 to 3.1 nm. A regular hexagonal assembly of nanoparticles can be seen in the TEM image. The triphenylene ligands play a crucial role in the self-assembly process. The distance between two GNPs was found to be about 4 nm, which is less than the ligand diameter indicating partial intercalation of the aliphatic chains, as shown in

figure 26. In the case of mixed monolayer covered GNPs (**18**) the TEM image (figure 27) show a random distribution of 2-4 nm size GNPs. ^{1}H NMR analysis of the product indicates the presence of triphenylene and hexanethiol moieties in 1:1 ratio.

The virgin TP-GNPs were found to be non-liquid crystalline. However, their doping in the columnar phase forming triphenylene-based DLCs does not disturb the nature of the mesophase. Binary mixtures of TP-GNPs and hexaheptyloxytriphenylene (H7TP) were prepared by sonicating the two components in dichloromethane followed by removal of the solvent and drying in vacuum. Three compositions (by weight) of TP-GNPs: H7TP (**19a**; 0.5 % TP-GNPs; **19b**; 1.0 % TP-GNPs and **19c**; 2.0 % TP-GNPs) were prepared and analyzed by differential scanning calorimetry (DSC) and polarizing optical microscopy (POM).

Table 5. Phase transition temperatures (peak, ºC) and associated enthalpy changes (KJ mol^{-1}, in parentheses of triphenylene-covered GNPs and H7TP composites. Cr = crystal, Col_h = hexagonal columnar mesophase, I = isotropic

Composite	Thermal transitions/°C	
	Heating scan	Cooling scan
H7TP	Cr 70 (61) Col_h 92.6 (5) I	I 90.2 (5) Col_h 46.8 (61) Cr
19a	Cr 68.9(61) Col_h 91.6 (3) I	I 89.3 (3) Col_h 46.4 (61) Cr
19b	Cr 69 (57) Col_h 91.0 (3) I	I 88.8 (3) Col_h 46.3 (60) Cr
19c	Cr 68.6 (58) Col_h 90.9 (4) I	I 87.4 (3) Col_h 42.4 (59) Cr

All the composites **19a**, **19b** and **19c** were found to be liquid crystalline in nature. They show classical textures of columnar mesophases upon cooling from the isotropic phase. A typical

texture of the mesophase obtained on cooling from the isotropic phase at 85 °C for **19c** is shown in figure 28. The DSC traces obtained on heating and cooling runs for **19c** are shown in figure 29. Data obtained from the heating and cooling cycles of DSC are collected in table 5.

A gradual decrease in the isotropic temperature upon increasing the amount of GNPs was observed. This is expected because of the insertion of the nanoparticles into the columnar matrix.

2.8.3.2 Thermogravimetric analysis (TGA)

The thermogravimetric analysis (TGA) of the TP-GNPs displays approximately 60% weight reduction at about 390 °C (figure 30), which may be attributed to the loss of the triphenylene units. From the TGA analysis of gold nanoparticles the composition ratio of TP-GNPs was estimated as gold: triphenylene thiol = 40: 60. To evaluate the mean composition of gold nanoparticle, we assumed a model with a 2.5 nm diameter for the gold nanosphere. Taking the gold core as a sphere with density ρ_{au} (58.01 atoms nm^{-3})[12] covered with a outermost layer of hexagonally close-packed gold atoms (13.89 atoms nm^{-2})[12] with a radius of R_{core} - R_{Au} (R_{Au} = 0.145 nm), the model predicts that the core contains about 420 gold atoms, of which 194 atoms lie on the surface. Furthermore from TGA, there are 147 of triphenylene thiol moieties at the surface of the 2.5 nm gold sphere. So the mean formula of TP-GNP nanoclusters is $Au_{420}(TP)_{147}$. The volume ratio of TP-GNPs in the H7TP matrix is found to be 1:12 based on the known structure of the columnar phase. In other words, while the mass percentage of TP-GNPs is 1 %, the volume occupied by the gold nanoparticle in the discotic matrix is considerably higher. This large volume of the TP-GNPs can only be present at the specific inter domain spacing to avoid disrupting the hexagonal order of H7TP as evidenced by our SAXS studies. The triphenylene molecules attached to gold nanoparticle interact with the H7TP molecules by van der Waals

interactions and are stabilized at the inter domain spaces. A schematic representation of the TP-GNPs in the columnar matrix of triphenylene-based DLCs is shown in figure 31.

2.8.3.3 X-ray diffraction studies (XRD)

The small angle X-ray diffraction patterns were recorded for composite **19b** and for pure H7TP under the same conditions at 75 °C. The diffraction pattern and the derived one-dimensional intensity *vs.* 2θ profile for pure H7TP and for the composite **19b** are shown in figure 32 (a, b) respectively. The overall features observed in both the cases are consistent with the structure of the Col_h phase. Figure 32(a) shows the SAXS pattern for the neat H7TP. The *d* values measured from the two peaks of the figure 32 (a) are in the ratio 1: $1/\sqrt{3}$ corresponding to the (1,0), (1,1) reflections from a two-dimensional hexagonal lattice with a *d* spacings of 18.72 Å. Figure 32 (b) shows the SAXS pattern for the nanocomposite. In this case also, we find that measured *d* values of the two peaks are in the ratio of 1: $1/\sqrt{3}$ corresponding to the (1,0), (1,1) reflections from a two-dimensional hexagonal lattice with a *d* spacings of 18.53 Å. This shows that the hexagonal order of the liquid crystal is not disturbed by the presence of gold nanoparticles in the nanocomposite. However, there is a very diffuse central dark band in figure 32 (b) around 33 Å arising due to the random distribution of TP-GNPs within the TP matrix in the nanocompisite. This indicated that the gold nanoparticles are distributed between the domain gaps in a random disordered manner.

2.8.3.4 DC conductivity

The DC conductivity studies of the H7TP and H7TP: TP-GNPs composites were carried out in indium tin oxide (ITO) coated glass sandwich cells (10mm x 5 mm) with a separation of 50 μm.

Current measurements were carried out using a Keithley pico ammeter (Model 480) along with a constant voltage source and a temperature controller. Figure 33 shows the DC conductivity values measured at different temperatures for pure H7TP and the mixture of 1% TP-GNPs and H7TP while cooling from isotropic temperature. There is a dramatic increase in DC conductivity by more than 10^6 times upon doping with 1 % TP-GNPs. The measured conductivity values also increase with increasing temperature. Changes in the slopes of the conductivity-temperature plots are observed for 1 % TP-GNP at 46 °C, indicative of a phase transition from crystalline to columnar mesophase.

The large electrical conductivity of the nanocomposites arises due to the highly delocalized π electron density of triphenylene molecules covalently bonded to gold nanoparticles which provide a facile path for electronic conduction. Previously, we have observed that the insertion of simple alkanethiol-covered GNPs into a columnar matrix enhanced the conductivity of the system by about 250 times. The enhanced electrical conductivity can be explained by an electron hoping mechanism [41] where the electrons tunnel from high electron density gold core to gold core along the nanoparticle array on the application of an electric field. The ability of gold nanoparticles to act as relay centers has been exploited earlier in photo-induced charge separation in gold nanoparticles, where an electron rich pyrene ligand acts as a donor and the gold nanoparticle as an acceptor [42]. The gold nanoparticles have also been shown to function as electron relays for connecting enzymes to a conductive substrate [43]. We suggest a similar mechanism operates in the case of nanocomposite, where electron rich triphenylene molecules act as a donor and the gold nanoparticle as the acceptor. The changes in the conductivity during phase transition are also indicative of more mobile charge carriers in the mesophase, which can be explained by less lateral interactions between H7TP and triphenylene ligands of GNP. We

therefore infer that these TP-GNP arrays, which are intercalated in the TP matrix, provide the necessary conducting path for the electron hopping, resulting in the enhanced conductivity of the composite.

2.8.4 Conclusions

In conclusions, we have reported here the synthesis of GNPs fully covered with triphenylene-based discotic liquid crystal, mixed monolayer with hexanethiol and dispersion of hexanethiol and triphenylene thiol-covered GNPs in a columnar matrix. POM, DSC and conductivity results indicate intercalation of TP-GNPs into the matrix of discotic liquid crystals. While a minor shift in the transition temperatures was observed, the nature of the mesophases is not disturbed in these compositions. They also exhibit enhanced electrical conductivity of more than six orders of magnitude compared to the corresponding neat triphenylene. The dispersion of discotic-capped nanoparticles in the liquid crystalline matrix can provide a route for synthesizing similar composites of varying properties that may find applications in many device developments.

2.9 Experimental

2.9.1 General information

Chemicals and solvents (AR quality) were used without any purification. All reactions were monitored by employing TLC technique using appropriate solvent system for development. Degassed solvents were used in the reaction involving oxygen sensitive materials. Transfer of moisture sensitive materials were carried out under N_2 atmosphere using standard syringe-septum techniques. All solvent extracts were washed successively with water, brine, and dried over anhydrous sodium sulphate and concentrated at reduced pressure on a Buchi rotary

evaporator. Yields reported are isolated yields of pure materials. The purity of all the compounds was confirmed from their homogeneous nature of a TLC plate, NMR spectrum and elemental analyses.

2.9.1.1 Column chromatography

Chromatographic separations were performed on silica gel (100-200 mesh).

2.9.1.2 Thin-layer chromatography

Thin-layer chromatography (TLC) was performed on aluminium sheets precoated with silica gel (Merck, Kieselgel 60, F254). Visualization of the spots on TLC plates was achieved by exposure to UV light.

2.9.1.3 Transition temperatures

The transition temperatures ans associated enthalpy values were determined using a differential scanning calorimeter (DSC, Perkin-Elmer, Model Pyris 1D) which was operated at a scanning rate 5 ºC/10 ºC min^{-1}. The apparatus was calibrated using indium (156.6 ºC) as a standard. Textural observation of the mesophase was carried out using polarizing optical microscopy (Olympus BX51) provided with a heating stage (Mettler FP82HT) and a central processor (Mettler FP 90).

2.9.1.4 X-ray diffraction studies

X-ray diffraction (XRD) was carried out in powder samples using using Cu-K_α (λ = 1.54 Å) radiation from a Rigaku ultrax 18 rotating anode generator (4 kW) monochromated with a

graphite crystal. The samples were held in sealed Lindemann capillary tubes (0.7 mm diameter) and the diffraction pattern were collected on a two-dimensional Marresearch image plate. A magnetic field of about 5 k Gauss was used to align the samples.

2.9.1.5 Ultraviolet spectra

Ultraviolet spectra recorded on UV-Visible Spectrophotometer (Hitachi U-3200).

2.9.1.6 IR spectra

IR spectra were recorded on Shimadzu FTIR-8400 spectrophotometer. IR spectra were obtained in Nujol mull for intermediate compounds and in KBr discs for the final compounds.

2.9.1.7 ^{1}H NMR & ^{13}C NMR

^{1}H NMR and ^{13}C NMR were recorded on a Brucker AMX 400 spectrometer. All chemical shifts were recorded in δ units downfield from Me_4Si, and *J* values are given in Hz.

2.9.1.8 Elemental analysis

Elemental analyses were performed on a Carlo-Erba 1106 analyser.

2.9.2 Synthesis

2.9.2.1 Synthesis of 6a (4'- [5-bromopentyloxy][1,1'-biphenyl]-4-carbonitrile)

A mixture of the **5** (0.5g, 2.56 mmol), 1, 5 dibromo hexane (2.94 g, 0.013 mol), Cs_2CO_3 (2.9 g, 0.009 mol), KI, and butanone was refluxed overnight. The mixture was allowed to cool to room temperature, the solids were filtered off and the solvent was evaporated under reduced pressure.

The oily residue was purified through a small column chromatography using 2 % ethyl acetate in hexane as an eluent. The residue was precipitated in methanol (five times the volume) and the crude product was filtered. It was again purified by crystallization from acetone:MeOH and CH_2Cl_2:hexane. The yield of the product was 750 mg (82 %).

^{1}H NMR (400 MHz, $CDCl_3$): δ 7.67 (d, *J* = 8.2 Hz, 2H), 7.61 (d, *J* = 8.2 Hz, 2H), 7.5 (d, *J* = 8.6 Hz, 2H), 6.9 (d, *J* = 8.6 Hz, 2H), 4.0 (t, *J* = 6.4 Hz, 2H), 3.5 (t, *J* = 7.1 Hz, 2H), 1.92-1.57 (m, 6H).

Elemental analysis: calculated for $C_{18}H_{18}BrNO$, C 62.8, H 5.27, N 4.07 %; found C 62.9, H 5.91, N 3.95 %.

2.9.2.2 Synthesis of 7a (4'- [(5-(acetylthio)-pentyl)oxy][1,1'-biphenyl]-4-carbonitrile)

Thioacetic acid (541 mg, 7.1 mmol) was added to a mixture of ethanol (50 ml) and Potassium tertiary butoxide (KO^tBu, 778 mg, 6.9 mmol)) and the mixture was stirred for 1 hour. 4'- [(5-bromopentyl)oxy][1,1'-biphenyl]-4-carbonitrile (**6a**, 2 g, 5.8 mmol) was added and the solution was refluxed for 24 hours. The cooled mixture was poured carefully onto dilute aqueous hydrochloric acid (50ml, 2 M) and extracted with dichloromethane (2 X 50 mL), the solvent was evaporated, and the product was purified by column chromatography [silica; dichloromethane-light petroleum (2:3)] to give 4'- [(5-(acetylthio)-pentyl)oxy][1,1'-biphenyl]-4-carbonitrile (**7a**) (1.1 g, 57 %) as a pale yellow solid.

^{1}H NMR (400 MHz, $CDCl_3$): δ 7.7 (d, *J* = 8.2 Hz, 2H), 7.6 (d, *J* = 8.2 Hz, 2H), 7.5 (d, *J* = 8.6 Hz, 2H), 6.9 (d, *J* = 8.6 Hz, 2H), 4.0 (t, *J* = 6.4 Hz, 2H), 2.9 (t, *J* = 7.1 Hz, 2H), 2.33 (s, 3H), 0.8-1.9 (m, 6H).

Elemental analysis: calculated for $C_{20}H_{21}NO_2S$**,** C 70.77, H 6.24, N 4.13, S 9.45 %; found C 71.22, H 6.55, N 4.10, S 9.15 %.

2.9.2.3 Synthesis of 9a (4'- [(5-sulphanylpentyl)oxy][1,1'-biphenyl]-4-carbonitrile)

Compound **7a** (100 mg) was dissolved in THF (5 ml) and the solution was degassed by bubbling N_2 for 5-10 minutes. A solution of $NaBH_4$ (45 mg) in 5 ml distilled water was added. The resulting mixture was kept at room temperature with stirring for 24 hours under nitrogen atmosphere. After that it was poured over distilled water and extracted with dichloromethane (3 X 25 ml). The combined organic extracts were washed with distilled water, dried over anhydrous sodium sulfate and evaporated to dryness under reduced pressure. The residue was purified by silica gel column chromatography (eluant: hexane-CH_2Cl_2, 1:1) to afford **9a** (84 mg, 95 %).

^{1}H NMR (400 MHz, $CDCl_3$): δ 7.7 (d, *J* = 8.2 Hz, 2H), 7.6 (d, *J* = 8.2 Hz, 2H), 7.5 (d, *J* = 8.6 Hz, 2H), 7.0 (d, *J* =8.6 Hz, 2H), 4.0 (t, *J* = 6.4 Hz, 2H), 2.6 (q, *J* =7.4 Hz, 2H), 1.2-1.9 (m, 7H).

^{13}C NMR (100 MHz, $CDCl_3$): 159.8, 145.3, 132.5, 131.4, 128.4, 127, 119, 115, 110, 68, 33.9, 29.7, 29.1, 28, 25.5.

Elemental analysis: calculated for $C_{18}H_{19}NOS$**,** C 72.69, H 6.44, N 4.71, S 10.78 %; found C 73.22, H 6.55, N 4.70, S 10.75 %.

IR data (KBr, all the derivatives **9a-9g** show similar spectrum) ν_{max} 2923.9, 2854.5, 2565.1, 2223.8, 1602.7, 1473.5, 1398.3, 1290.3, 1245.9, 1180.4, 1012.6, 827.4 cm^{-1}.

UV-Vis data ($CHCl_3$, all the derivatives **9a-9g** show similar spectrum): λ_{max} 331 nm.

4'- [(6-sulphanylhexyl)oxy][1,1'-biphenyl]-4-carbonitrile (9b).

^{1}H NMR (400 MHz, $CDCl_3$): δ 7.7 (d, *J* = 8.2 Hz, 2H), 7.6 (d, *J* = 8.2 Hz, 2H), 7.5 (d, *J* = 8.6 Hz, 2H), 6.9 (d, *J* = 8.6 Hz, 2H), 4.0 (t, *J* = 6.4 Hz, 2H), 2.7 (q, *J* =7.4 Hz, 2H), 1.3-1.9 (m, 9H).

Elemental analysis: calculated for $C_{19}H_{21}NOS$**,** C 73.27, H 6.80, N 4.50, S 10.30 %; found C 72.84, H 7.22, N 4.52, S 10.26 %.

4'- [(7-sulphanylheptyl)oxy][1,1'-biphenyl]-4-carbonitrile (9c).

^{1}H NMR (400 MHz, $CDCl_3$): δ 7.7 (d, *J* = 8.2 Hz, 2H), 7.6 (d, *J* = 8.2 Hz, 2H), 7.5 (d, *J* = 8.6 Hz, 2H), 6.9 (d, *J* = 8.6 Hz, 2H), 4.0 (t, *J* = 6.4 Hz, 2H), 2.7 (q, *J* = 7.4 Hz, 2H), 1.3-1.9 (m, 11H).

Elemental analysis: calculated for $C_{20}H_{23}NOS$**,** C 73.81, H 7.12, N 4.30, S 9.85 %; found C 74.30, H 7.46, N 4.79, S 9.67 %.

4'- [(8-sulphanyloctyl)oxy][1,1'-biphenyl]-4-carbonitrile (9d).

^{1}H NMR (400 MHz, $CDCl_3$): δ 7.7 (d, *J* = 8.2 Hz, 2H), 7.6 (d, *J* = 8.2 Hz, 2H), 7.5 (d, *J* = 8.6 Hz, 2H), 6.9 (d, *J* = 8.6 Hz, 2H), 4.0 (t, *J* = 6.4 Hz, 2H), 2.7 (q, *J* = 7.4 Hz, 2H), 1.3-1.9 (m, 13H).

Elemental analysis: calculated for $C_{21}H_{25}NOS$**,** C 74.29, H 7.42, N 4.13, S 9.45 %; found C 73.84, H 7.65, N 4.11, S 9.20 %.

4'- [(9-sulphanylnonyl)oxy][1,1'-biphenyl]-4-carbonitrile (9e).

^{1}H NMR (400 MHz, $CDCl_3$): δ 7.7 (d, *J* = 8.2 Hz, 2H), 7.6 (d, *J* = 8.2 Hz, 2H), 7.5 (d, *J* = 8.6 Hz, 2H), 6.9 (d, *J* = 8.6 Hz, 2H), 4.0 (t, *J* = 6.4 Hz, 2H), 2.7 (q, *J* = 7.4 Hz, 2H), 1.3-1.9 (m, 15H).

Elemental analysis: calculated for $C_{22}H_{27}NOS$**,** C 74.74, H 7.70, N 3.96, S 9.07 %; found C 74.47, H 7.85, N 4.27, S 8.73 %.

4'- [(10-sulphanyldecyl)oxy][1,1'-biphenyl]-4-carbonitrile (9f).

^{1}H NMR (400 MHz, $CDCl_3$): δ 7.7 (d, *J* = 8.2 Hz, 2H), 7.6 (d, *J* = 8.2 Hz, 2H), 7.5 (d, *J* = 8.6 Hz, 2H), 6.9 (d, *J* = 8.6 Hz, 2H), 4.0 (t, *J* = 6.4 Hz, 2H), 2.7 (q, *J* = 7.4 Hz, 2H), 1.3-1.9 (m, 17H).

Elemental analysis: calculated for $C_{23}H_{29}NOS$**,** C 75.16, H 7.95, N 3.81, S 8.72 %; found C 74.75, H 7.80, N 3.50, S 8.40 %.

4'- [(12-sulphanyldodecyl)oxy][1,1'-biphenyl]-4-carbonitrile (9g).

^{1}H NMR (400 MHz, $CDCl_3$): δ 7.7 (d, *J* = 8.2 Hz, 2H), 7.6 (d, *J* = 8.2 Hz, 2H), 7.5 (d, *J* = 8.6 Hz, 2H), 6.9 (d, *J* = 8.6 Hz, 2H), 4.0 (t, *J* = 6.4 Hz, 2H), 2.7 (q, *J* = 7.4 Hz, 2H), 1.3-1.9 (m, 21H).

Elemental analysis: calculated for $C_{25}H_{33}NOS$**,** C 75.90, H 8.41, N 3.54, S 8.11 %; found C 74.30, H 8.37, N 3.00, S 7.50 %.

References

[1] R. Narayanan, M. A. El-Sayed, *J. Phys. Chem. B*, **109**, 12663 (2005).

[2] R. Elghanian, J. J. Storhoff, R. C. Mucic, R. L. Letsinger, C. A. Mirkin, *Science*, **277**, 1078 (1997).

[3] A. P. Alivisatos, K. P. Johnsson, X. Peng, T. E. Wislon, C. J. Loweth, M. P. Bruchez, P. G. Schultz, *Nature*, **382**, 609 (1996).

[4] M. Brust, M. Walker, D. Bethell, D. J. Schiffrin, R. Whyman, *J. Chem. Soc., Chem. Commun*., 801 (1994).

[5] It would be impossible to report all the studies dealing with the chemistry and physics of gold nanoparticles. For a very recent review and papers, see: (a) M. –C. Daniel, D. Astruc, *Chem. Rev*., **104**, 293 (2004). (b) S. Eustis, M. A. El-Sayed, *Chem. Soc. Rev*., **35**, 209 (2006). (c) O. Abed, M. Wanunu, A. Vaskevich, R. Arad-Yellin, A. Shanzer, I. Rubinstein, *Chem. Mater*., **18**, 1247 (2006). (d) J. –E, Park, M. Atobe, T. Fuchigami, *Ultrasonics Sonochemistry*, **13**, 237 (2006). (e) Z. Zhang, F. Wang, F. Chen, G. Shi., *Mater. Lett*., **60**, 1039 (2006). (f) X. Hu, Q. Zhao, X. Jiang, C. Zhu, J. Qiu., *Solid State Commun*., **138**, 43 (2006). (g) J. Chen, J. Tang, F. Yan, H. Ju, *Biomaterials*, **27**, 2313 (2006). (h) S. F. Sweeney, G. H. Woehrle, J. E. Hutchison, *J. Am. Chem. Soc*., **128**, 3190 (2006). (i) Y. Ma, L. Qian, H. Huang, X. Yang, *J. Colloid. Int. Sci*., **295**, 583 (2006). (j) L. B. Scaffardi, J. O. Tocho, *Nanotechnology*, **17**, 1309 (2006). (k) M. Sakamoto, T. Tachikawa, M. Fujitsuka, T. Majima, *Chem. Phys. Lett*., **420**, 90 (2006). (l) M. S. Vickers, J. Cookson, P. D. Beer, P. T. Bishop, B. Thiebaut, *J. Mater. Chem*., **16**, 209 (2006). (m) Y. Y. Xu, C. Bian, S. Chen, S. Xia, *Analytica Chimica Acta*, **561**, 48 (2006). (n) B. Nie, M. R. Shortreed, L. M. Smith, *Analytical Chem*., **78**, 1528 (2006). (o) S. –W.

Joo, *Spectroscopy letters*, **39**, 85 (2006). (p) Y. Ding, X. Zhang, X. Liu, R. Guo, *Langmuir*, **22**, 2292 (2006). (q) Z. Wang, R. Levy, D. G. Fernig, M. Brust., *J. Am. Chem. Soc*., **128**, 2214 (2006). (r) B. I. Ipe, K. Yoosaf, K. G. Thomas, *J. Am. Chem. Soc*., **12**8, 1907 (2006). (s) R. Bhattacharya, C. R. Patra, S. Wang, L. Lu, M. J. Yaszemski, D. Mukhopadhyay, P. Mukherjee, *Adv. Func. Mater*., **16**, 395 (2006). (t) C. M. Welch, R. G. Compton, *Analytical and Bioanalytical Chem*., **384**, 601 (2006). (u) J. Sharma, R. Chhabra, Y. Liu, Y. Ke, H. Yan, *Angew. Chem*., **45**, 730 (2006). (v) J. Shan, J. Chen, M. Nuopponen, T. Viitala, H. Jiang, J. Peltonen, E. Kauppinen, H. Tenhu, *Langmuir*, **22**, 794 (2006). (w) I.-Im. S. Lim, J. Ouyang, J. Luo, L. Wang, S. Zhou, C. –J. Zhong, *Chem. Mater*., **17**, 6528 (2005). (x) T. Hasobe, H. Imahori, P. V. Kamat, T. K. Ahn, S. K. Kim, D. Kim, A. Fujimoto, T. Hirakawa, S. Fukuzumi, *J. Am. Chem. Soc*., **127**, 1216 (2005).

[6] (a) J. Qiu, X. Jiang, C. Zhu, M. Shirai, J. Si, N. Jiang, K. Hirao, *Angew. Chem. Int. Ed*., **43**, 2230 (2004). (b) J. M. Kinyanjui, D. W. Hatchett, *Chem Mater*., **16**, 3390 (2004). (c) H –Li. Zhang, S. D. Evans, J. R. Henderson, R. E. Miles, T. Shen, *J. Phys. Chem. B*, **107**, 6087 (2003). (d) A. Swami, A. Kumar, P. R. Sevekannan, S. Mandal, M. Saatry, *J. Colloid Interface Sci*., **260**, 367 (2003). (e) K. Sato, K. Hosokawa, M. Maeda, *J. Am. Chem. Soc*., **125,** 8102 (2003). (f) C. K. Yee, A. Ulman, J. D. Ruiz, A. Parikh, H. White, M. Rafailovich, *Langmuir*, **19**, 9450 (2003). (g) I. Sondi, D. V. Goia, E. Matijevic, *J. Colloid Int. Sci*., **260**, 75 (2003). (h) M. Zheng, F. Davidson, X. Huang, *J. Am. Chem. Soc*., **125**, 7790 (2003). (i) Y. Tan, Y. Li, D. Zhu, *J. Colloid. Int. Sci*., **258**, 244 (2003). (k) D. Li, Y. Zhang, J. Jiang, J. Li, *J. Colloid. Int. Sci*., **264**, 109 (2003). (l) M. Hasan, D. Bethell, M. Brust., *J. Am. Chem. Soc*., **124**, 1132 (2002). (m) C. Mangency, F. Ferrage, I. Aujard, V. M- Artzner, L. Jullien, O. Ouari, Ei. D. Rekhai, A. Laschewasky, I. Vikholm,

J. W. Sadowski, *J. Am. Chem. Soc*., **124**, 5811 (2002). (n) T-Quyen. Nguyen, M. L. Bushby, L. E. Brus, C. Nuckolls, *J. Am. Chem. Soc*., **124**, 15051 (2002). (o) N. R. Jana, L.A. Gearherat, S.O. Obare, C. J. Johnson, K. J. Edler, S. Mann, C. J. Murphy, *J. Mater. Chem*., **12**, 2902 (2002). (p) A. B. Lowe, B. S. Sumerlin, M. S. Donovan, C. L. McCormick, *J. Am. Chem. Soc*., **124**, 11562 (2002). (q) M. K. Corbierre, N. S. Cameron, M. Sutton, S. G. J. Mochrie, L. B. Lurio, A. Ruhm, R. Bruce Lennox, *J. Am. Chem. Soc*., **123**, 10411 (2001). (r) Y. Wei Cao, R. Jin, C. A. Mirkin, *J. Am. Chem. Soc*., **123**, 7961 (2001). (s) J. Hu, J. Zhang, F. Liu, K. Kittredge, J. K. Whitesell, M. Anne Fox, *J. Am. Chem Soc*., **123**, 1464 (2001). (t) W. W. Weare, S. M. Reed, M. G. warner, J. E. Hutchison, *J. Am. Chem. Soc*., **122**, 12890 (2000). (u) M. Green, P. O'Brien, *Chem. Commun*., 183 (2000). (v) J. Simard, C. Briggs, A. K. Boal, V. M. Rotello, *Chem Commun*., 1943 (2000). (w) J. Schmitt, P. Machtle, D. Eck, H. Mohwald, C. A. Helm, *Langmuir*, **15**, 3256 (1999). (x) V. Patil, R. B. Malvankar, Murali Sastry, *Langmuir*, **15**, 8197 (1999). (y) A. C. Templeton, S. Chen, S. M. Gross, R. W. Murray, *Langmuir*, **15**, 66 (1999). (z) D. Fitzmaurice, S. Nagaraja Rao, J. A. Preece, J. Fraser Stoddart, S. Wenger, N. Zaccheroni, *Angew. Chem. Int. Ed*., **38,** 1147 (1999).

[7] (a) S. Chen, K. Kimura, *Langmuir*, **15**, 1075 (1999). (b) X. M. Lin, C. M. Sorensen, *Chem. Mater*., **11**, 198 (1999). (c) S. R. Johnson, S. D. Evans, R. Brydson, *Langmuir*, **14**, 6639 (1998). (d) J. Fink, C. J. Kiely, D. Bethell, D. J. Schiffrin, *Chem. Mater*., **10**, 922 (1998). (e) M. J. Hostetler, J. E. wingate, C-Jian Zhong, J. E. Harris, R. W. Vachet, M. R. Clark, J. David Londono, S. J. Green, J. J. Stokes, G. D. Wignall, G. L. Glish, M. D. Porter, N. D. Evans, R. W. Murray, *Langmuir*, **14**, 17 (1998). (f) A. C. Templeton, M. J. Hostetler, C. T. Kraft, R. W. Murray, *J. Am. Chem. Soc*., **120**, 1906 (1998). (h) S. R.

Johnson, S. D. Evans, S. W. Mahon, A. Ulman, *Langmuir*, **13,** 51 (1997). (i) K-Sub. Kim, S. Choi, J. –H Cho, S. –Hwa, H. Lee, *J. Mater. Chem*., **16**, 1315 (2006). (j) L. Cseh, G. H. Mehl, *J. Am. Chem. Soc*., **128**, 13376 (2006). (k) A. I. Abdelrahman, A. M. Mohammad, T. Okajima, T. Ohsaka, *J. Phys. Chem. B*, **110**, 2798 (2006).

[8] T. Ikeda, O. Tsutsumi, *Science*, **268**, 1873 (1995).

[9] (a) M. Giersig, P. Mulvaney, *J. Phys. Chem*., 97, 6334 (1993). (b) J. H. Fendler, *Chem. Mater*., **8**, 1616 (1996).

[10] (a) J. J. Storhoff, C. A. Miirkin, *Chem. Rev*., **99**, 1849 (1999). (b) S. Mann, W. Shenton, M. Li, S. Connolly, D. Fitzmaurice, *Adv. Mater*., **12**, 147 (2000).

[11] Y. Song, T. Huang, R. W. Murray, *J. Am. Chem Soc*., **125**, 11694 (2003).

[12] H. Schonheer, F. J. B. Kremer, S. Kumar, J. A. Rego, H. Wolf, H. Ringsdorf, M. Jaschke, H. Butt, E. Bamberg, *J. Am. Chem. Soc*., **118,** 13051 (1996).

[13] S. Kumar, S. K. Varshney, *Synthesis*, 305 (2001).

[14] S. Kumar, S. K. Varshney, *Angew. Chem. Int. Ed*., **39**, 3140 (2000).

[15] (a) G. W. Gray, K. J. Harrison, J. A. Nash. *Electron. Lett*., **9**, 130 (1973). (b) G. W. Gray, K. J. Harrison, J. A. Nash, J. Constant, J. S. Hulme, J. Kirton, E. P. Raynes, *Liquid Crystals and Oriented Fluids*, vol. 2, R. S. Porter, J. F. Johnson (eds.), p. 617, Plenum, New York (1973).

[16] (a) D. A. Dunmur, A. Fukada, G. R. Luckhrust (editors), *Physical Properties of Liquid Crystals: Nematics*. INSPEC, London (2001) (b) D. Demus, J. Goodby, G. W. Gray, H. –W. Spiess and V. Vill (editors). *Hand Book of Liquid Crystals*, vols. 1 and 2, Wiley-VCH, weinheim (1998).

[17] (a) G. S. Attard, C. T. Imrie, F. E. Karasz. *Chem. Mater*., **4**, 1276 (1992). (b) G. S. Attard, R. W. Date, C. T. Imrie, G. R. Luckhrust, S. J. Roskilly, J. M. Seddon, L. Taylor. *Liq. Cryst*., **16**, 529 (1994). (c) Y. Kawakami, M. Baba, Y. Murate, H. Kunisada, Y. Yuki. *Polym. J*., **28**, 1006 (1996). (d) W. Weissflog, D. Demus, S. Diele, P. Nitschke, W. Wedler. *Liq. Cryst*., **5**, 111 (1989). (e) A. C. Griffin, S. R. Vaidya, *Mol. Cryst. Liq. Cryst*., **173**, 85 (1989). (f) V. Percee, M. Lee. *Macromolecules*, **24**, 1017 (1991). (g) V. Percee, M. Lee, *J. Macromol. Sci. Chem*., **28**, 651 (1991). (h) V. Percee, M. Lee, A. Ackerman, *Polymer*, **33**, 703 (1992). (h) P. Zugennmaier, A. Heiske, *Liq. Cryst*., **15**, 835 (1993). (i) T. Shibata, M. Kimura, S. Takano, K. ogasawara. *Mol. Cryst. Liq. Cryst*., **237**, 483 (1993). (j) P. A. G. Cormack, B. D. Moore, D. C. Sherrington, *J. Mater. Chem*., **7**, 1977 (1997). (k) A. Omenat, J. Lub, H. Fischer, *Chem. Mater*., **10**, 518 (1998). (l) K. M. Kim, Y. Chujo, *J. Polym. Sci. polym. Chem*., **39**, 4035 (2001). (m) L. C. Chien, L. G. Cada, L. Xie, *Liq. Cryst*., **12**, 853 (1992). (n) M. Kawasumi, A. Usuki, A. Okada, T. Kurauchi, *Mol. Cryst. Liq. Cryst*., **281**, 91 (1996). (o) H. Budig, S. Diele, P. Goring, R. Paschke, C. Sauer, C. Tschierske, *J. Chem. Soc., Perkin Trans. II*, 767 (1995). (p) R. Lunkwitz, C. Tschierske, S. Diele, *J. Mater. Chem*., **7**, 2001 (1997). (q) P. A. Tuan, S. G. Kostromin, V. P. Shibave, *Polym. Bull*., **29**, 49 (1992). (r) P. A. Gemmel, G. W. Gray, D. Lacey, *Mol. Cryst. Liq. Cryst*., **122**, 205 (1985). (s) D. Braun, N. Arnold, A. Liebmann, I. Schmidtke, *Makromol. Chem*., **194**, 2687 (1993). (t) J. Newton, H. Coles, P. Hodge, J. Hannington, *J. Mater. Chem*., **4**, 869 (1994). (u) G. H. Mehl, J. W. Goodby, *Mol. Cryst. Liq. Cryst*., **303**, 15 (1997).

[18] See, for example, C. T. Imrie, *Structure and Bonding*, D. M. P. Mingos (Ed.), p. 149, Springer-Verlag, Berlin (1999). (b) C. T. Imrie, G. R. Luckhurst, *Hand Book Of Liquid*

Crystals, Vol. 2B, D. Demus, J. Goodby, G. W. Gray, H.-W. Spiess, V. Vill (Eds), Chap. X. Wiley-VCH, Weinheim (1998). (c) I. D. Fletcher, G. R. Luckhurst, *Liq. Cryst*., **18**, 175 (1995). (d) N. Koide, H. Iida, *Mol. Cryst. Liq. Cryst*., **261**, 427 (1995). (e) M. Kijima, K. Akagi, H. Shirakawa, *Synth. Met*., **84**, 237 (1997). (f) P. J. Langlev, F. J. Davis, G. R. Mitchell, *Mol. Cryst. Liq. Cryst*., **236**, 225 (1993). (g) M. D. Everaars, A. T. M. Marcelis, E. J. R. Sudholter, *Thin Solid Films*, **242**, 78 (1994). (h) D. Joachimi, C. Tschierske, H. Muller, J. H. Wendorff, L. Schneider, R. Kleppinger, *Angew. Chem*., **105**, 1205 (1993). (i) P. H. J. Kouwer, C. J. Welch, G. MaRobbie, B. J. Dodds, L. Priest, G. H. Mehl, *J. Mater. Chem*., **14**, 1798 (2004). (j) I. M. Saez, J. W. Goodby, *Liq. Cryst. Today*, **13**, 1 (2004).

[19] G. S. Attaed, R. W. Date, C. T. Imrie, G. R. Luckhurst, S. J. Roskilly, J. M. Seddon, L. Taylor, *Liq. Cryst*., **16**, 529 (1994).

[20] M. Hird, *Physical Properties of Liquid Crystals: Nematics*, D. A. Dunmur, A. Fukuda, G. R. Luckhurst (Eds), Chap. 1.1, INSPEC, London (2001).

[21] (a) A. Ulman, *An Introduction to Ultrathin Organic Flims from Langmuir-Blodgett to Self-Assembly*, Academic Press, San Diego, CA, (1991). (b) H. O. Finklea, In R. A. Meyers (ed.), *Encyclopedia of Analytical Chemistry*, Wiley, Chichester, (2000).

[22] H. O. Finklea, In: A Bard, I. Rubinstein (Eds.), *Electroanalytical Chemistry*, vol. 19, Dekker, New York, (1996).

[23] (a) S. S. Wong, M. D. Porter, *J. Electroanal. Chem*., **485**, 135 (2000). (b) F. Schreiber, *Prog. Surf. Sci*., **65**, 151 (2000). (c) C. E. D. Chidsey, C. R. Bertozzi, T. M. Putvinski, A. M. Musjsce, *J. Am. Chem. Soc*., **112**, 4301 (1990). (d) A. M. Becka, C. J. Miller, *J. Phys. Chem*., **97**, 6233 (1993).

[24] (a) M. J. Tariov, D. R. F. Burgess, G. Gillen, *J. Am. Chem. Soc*., **115**, 5305 (1993). (b) J. Huang, D. A. Dahlgren, J. C. Hemminger, *Langmuir*, **10**, 626 (1994). (c) E. W. Wollman, D. Kang, C. D. frisbie, T. M. Larcovic, M. S.. Wrighton, *J. Am. Chem. Soc*., **116**, 4395 (1994).

[25] (a) J. J. Hickman, D. Ofer, P. E. Laibinis, G. M. Whitessides, *Science*, **252**, 688 (1991). (b) C. A. Mirkin, M. A. Ratner, *Annu. Rev. Phys. Chem*., **43**, 719 (1992). (c) C. J. Zhong, M. D. Porter, *Anal. Chem*., **67**, 709A (1995). (d) B. A. Cornell, V. L. B. Braach-Maksvytis, L. G. King, P. D. J. Osman, B. Raguse, L. Wieczorek, R. J. Pace, *Nature*, **387**, 580 (1997).

[26] D. Li, M. A. Ratner, T. J. Marks, C. H. Znang, J. Yang, G, K. Wong, *J. Am. Chem. Soc*., **112**, 7389 (1990).

[27] Y. Xia, G. M. Whitesides, *Angew. Chem. Int. Ed*., **37**, 550 (1998).

[28] (a) Y. Xiao, F. Patolsky, E. Katz, J. F. Hainfeld, I. Willner, *Science*, **299**, 1877 (2003). (b) F. R. F. Fan, J. P. Yang, L.T. Cai, D. W. Price, S. M. Dirk, D. V. Kosynkin, Y. X. Yao, A. M. rawlett, J. M. Tour, A. J. Bard, *J. Am. Chem. Soc*., **124**, 5550 (2002). (c) M. Aslam, N. K. Chaki, J. Sharma, K. Vijayamohanan, *Curr. Appl. Phys*., **3**, 115 (2003).

[29] Y. Kawanishi, T. Tamaki, M. Sakuragi, T. Seki, Y. Swuzki, K. Ichimura, *Langmuir*, **8**, 2601 (1992).

[30] (a) P. E. Laibinis, G. M. Whitesides, *J. Am. Chem. Soc*., **114**, 9022 (1992). (b) N. Ohno, J. Uehara, K. Aramaki, *J. Electrochem. Soc*., **140**, 2512 (1993).

[31] (a) C. E. D. Chidsey, *Science*, **251**, 919 (1999). (b) H. D. Sikes, J. F. Smalley, S. P. Dudek, A. R. Cook, M. D. Newton, C. E. D. Chidsey, S. W. Feldberg, *Science*, **291**, 1519 (2001). (c) T. Felgenhauer, H. T. Rong, M. Buck, *J. Electroanal. Chem*., **550**, 309 (2003).

[32] (a) U. K. Sur, R. Subramanian, V. Lakshminarayanan, *J. Colloid Interface Sci*., **266**, 175 (2003). (b) R. P. Janek, W. R. Fawcett, A. Ulmann, *Langmuir*, **14**, 3011 (1998). (c) L. V. Protsailo, W. R. Fawcett, *Langmuir*, **18**, 8933 (2002).

[33] (a) H. O. Finklea, L. Liu, M. S. ravenscroft, S. Punturi, *J. Phys. Chem*., **10**, 18852 (1996). (b) H. O. Finklea, D. D. Hanshew, *J. Am.Chem. Soc*., **114**, 3173 (1992). (c) M. E. G. Lyons, *Sensors*, **1**, 215 (2001). (d) S. Nitahara, T. Akiyama, S. Inoue, S. Yamada, *J. Phys. Chem. B*, **109**, 3944 (2005). (e) M. R. Arkin, E. D. A. Stemp, C. Turro, N. J. Turro, J. K. Barton, *J. Am. Chem. Soc*., **118**, 2267 (1996). (f) D. Meisel, M. S. Matheson, J. Rabani, *J. Am. Chem. Soc*., **100**, 117 (1978).

[34] (a) E. Sabatani, J. Cohen-Boulakia, M. Bruening, I. Rubinstein, *Langmuir*, **9**, 2974 (1993). (b) A. W. Hayes, C. Shannon, *Langmuir*, **12**, 3688 (1996). (c) M. A. Rampi, G. M. Whitesides, *Chem. Phys*., **281**, 373 (2002). (d) D. J. World, R. Hagg, M. A. Rampi, C. D. Frisbie, *J. Phys. Chem. B*, **106**, 2813 (2002).

[35] (a) P. Cyganik, M. Buck, W. Azzam, C. Woll, *J. Phys. Chem. B*, **108**, 4989 (2004). (b) Y. T. Long, H. T. Rong, M. Buck, M. Grunze, *J. Electroanal. Chem*., **524-525**, 62 (2002). (c) J. F. Kang, A. Ulman, S. Liao, R. Jordan, *Langmuir*, **15**, 2095 (1999).

[36] (a) See, for example, H. Schonheer, F. J. B. Kremer, S. Kumar, J. A. Rego, H. Wolf, H. Ringsdorf, M. Jaschke, H. Butt, E. Bamberg, *J. Am. Chem. Soc*., **118**, 13051 (1996). (b) N. Boden, R. J. Bushby, P. S. Martin, S. D. Evans, R. W. Owens, D. A. Smith, *Langmuir*, **15**, 3790 (1999). (c) R. Owens, D. A. Smith, *Mol. Cryst. Liq. Cryst*., **329**, 427 (1999). (d) H. Allinson, N. Boden, R. J. Bushby, S. D. Evans, P. S. Martin, *Mol. Cryst. Liq. Cryst*., **303**, 273 (1997). (e) Z. P. Yang, I. Engquist, J. M. Kauffmann, B. liedberg, *Langmuir*, **12**, 1704 (1996). (f) Y. T. Tao, M. T. Lee, *Thin solid Flims*, **244**, 810 (1994).

[37] V. Ganesh, S. K. Pal, S. Kumar, V. Lakshminarayanan, *J. Colloid. Int. Sci*., **296**, 195 (2006).

[38] V. Ganesh, S. K. Pal, S. Kumar, V. Lakshminarayanan, *Electrochimica Acta*, **52**, 2987 (2007).

[39] I. In, Y-W. Jun, J. Kim, S. Y. Kim, *Chem Commun*, 801 (2005).

[40] (a) S. Kumar, M. Manickam, *Chem Commun*., 1615 (1997). (b) S. Kumar, M. Manickam, *Synthesis*, 1119 (1998). (c) S. Kumar, J. J. Naidu, S. K. Varshney, *Mol. Cryst. Liq. Cryst*., **411**, 355 (2004).

[41] R. H. Terrill, T. A. Postlethwaite, C. –H. Chen, C. –D. Poon, A. Terzis, A. Chen, J. E. Hutchison, M. R. Clark, G. Wignall, J. D. Londono, R. Superfine, M. Falvo, C. S. Johnson, Jt., E. T. Samulski, R. W. Murray, *J. Am. Chem. Soc*., **117**, 12537 (1995).

[42] I. Ipe, K. G. Thomas, S. Barazzouk, S. Hotchandani, P. V. Kamat, *J. Phys. Chem. B*, **106**, 18 (2002).

[43] F. Y. Xiao, F. Patolsky, E. Katz, J. F. Hainfeld, I. Wilner, *Science*, **299**, 1877 (2003).

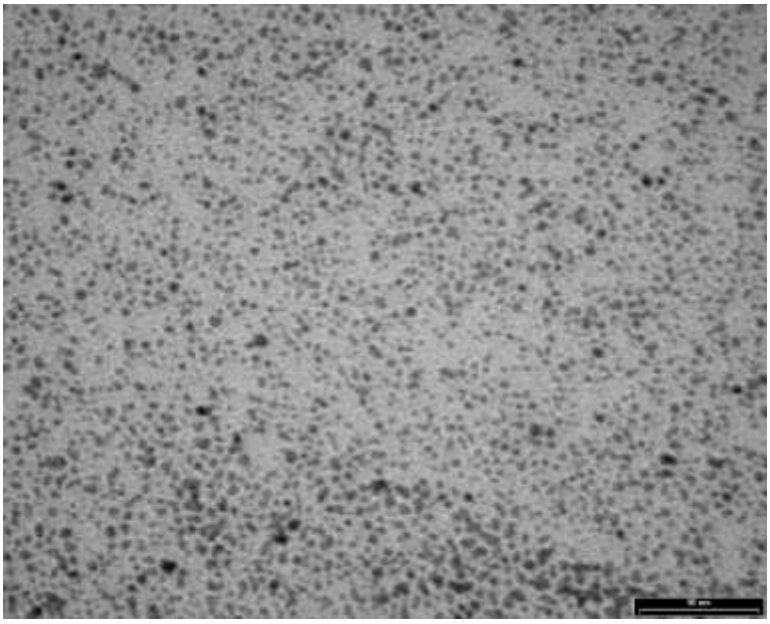

Figure 1. TEM image of hexane-thiol capped gold nanoparticles

.

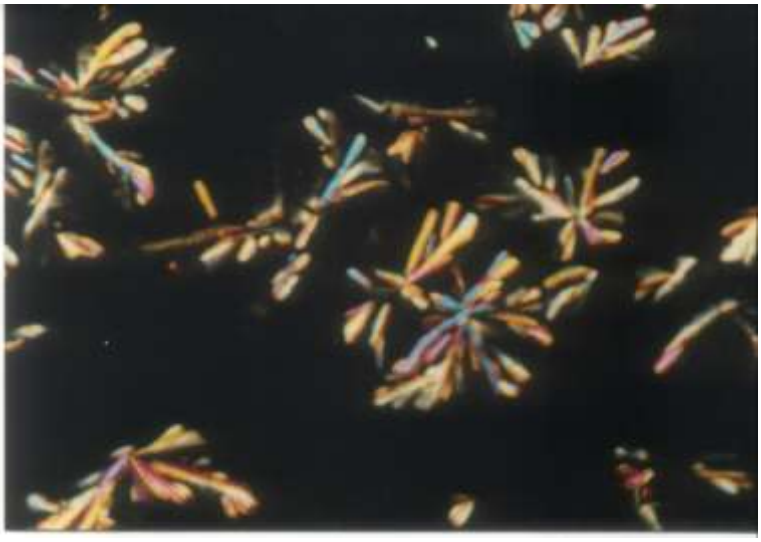

Figure 2. POM photograph of the columnar phase of **3c** at 83 °C (crossed polarizers, magnification X 200).

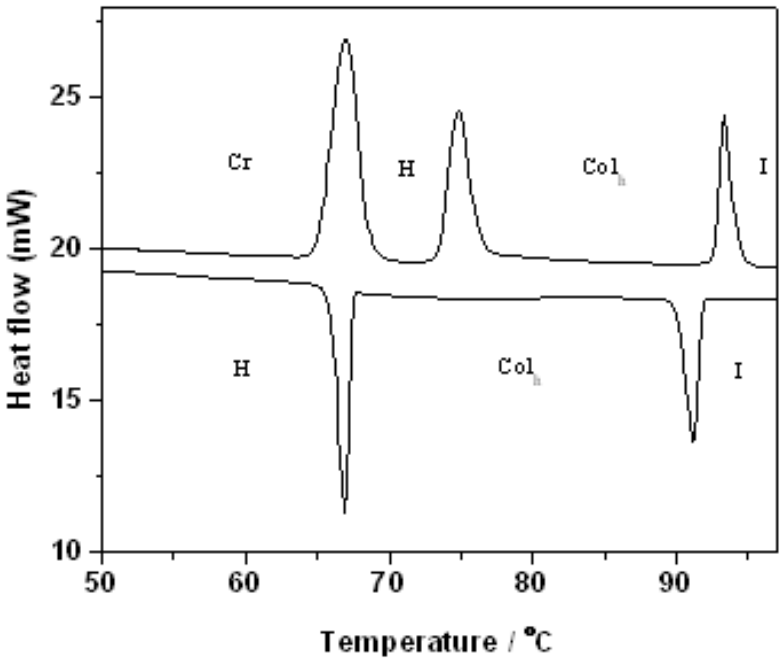

Figure 3. DSC traces for compound **2** on heating and cooling (scan rate 10 °C min^{-1}).

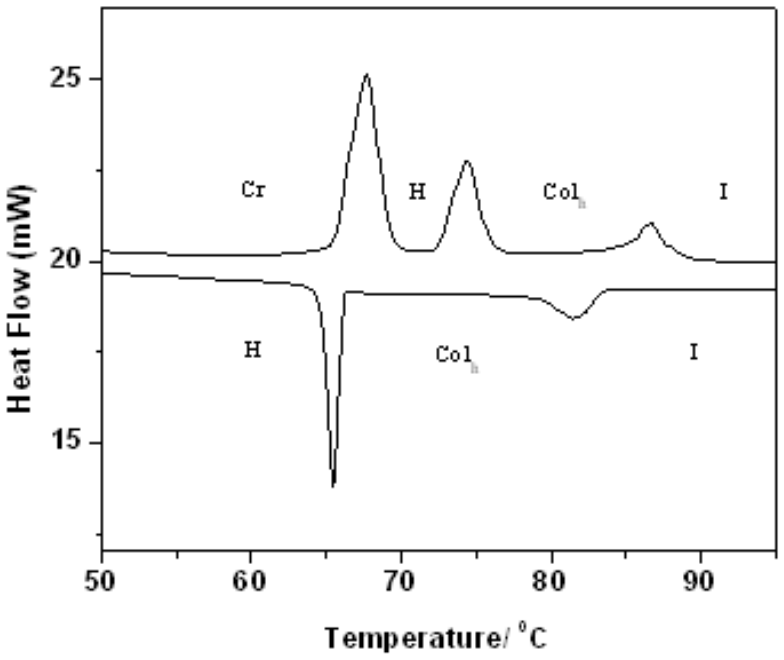

Figure 4. DSC traces for composite **2a** on heating and cooling (scan rate 10 °C min^{-1})

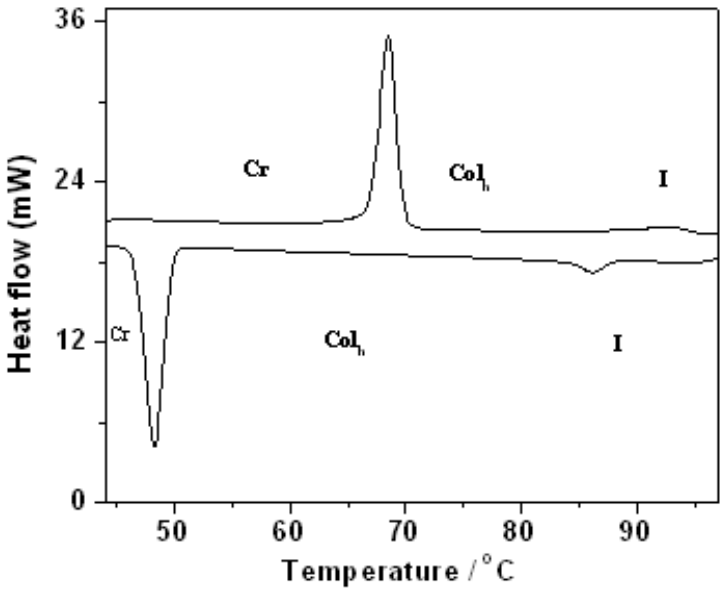

Figure 5. DSC traces for composite **3c** on heating and cooling (scan rate 10 °C min^{-1})

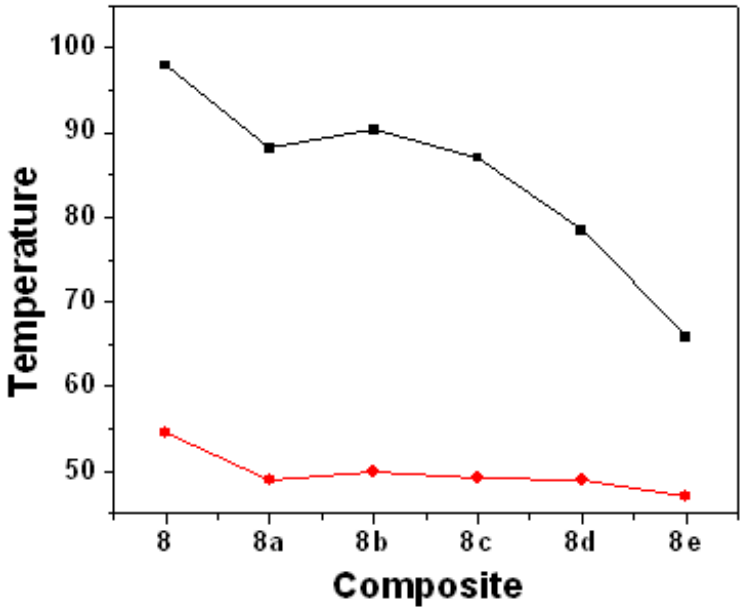

Figure 6. Transition temperatures of GNP-H6T composites.

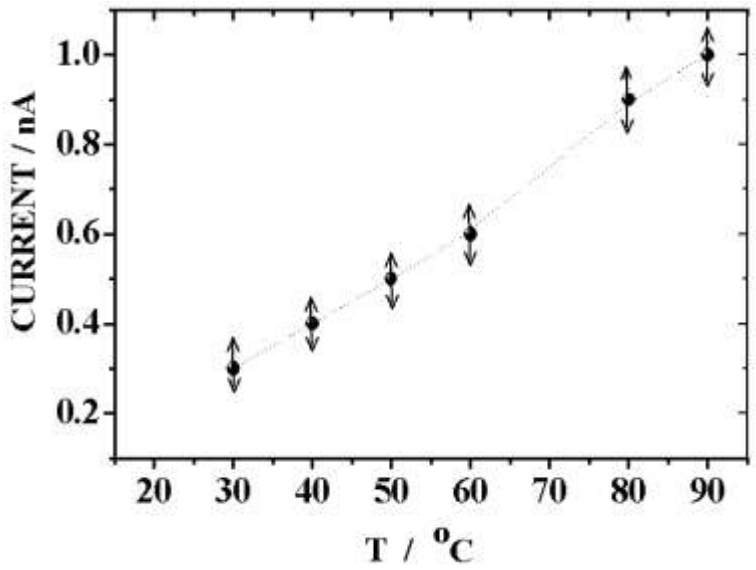

Figure 7. Plot of variation of current with temperature in GNP-HHTT (1:1) composite.

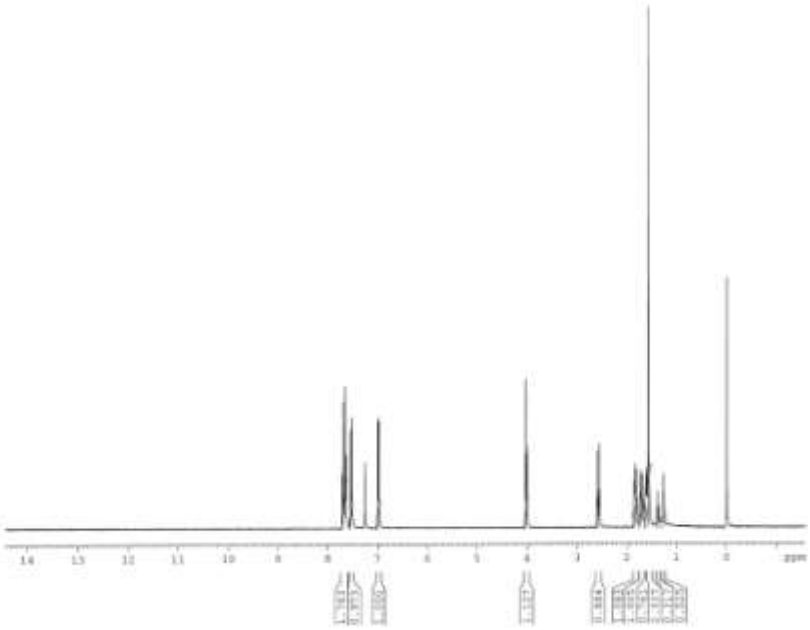

Figure 8. ^{1}H NMR spectrum of the compound **9a**.

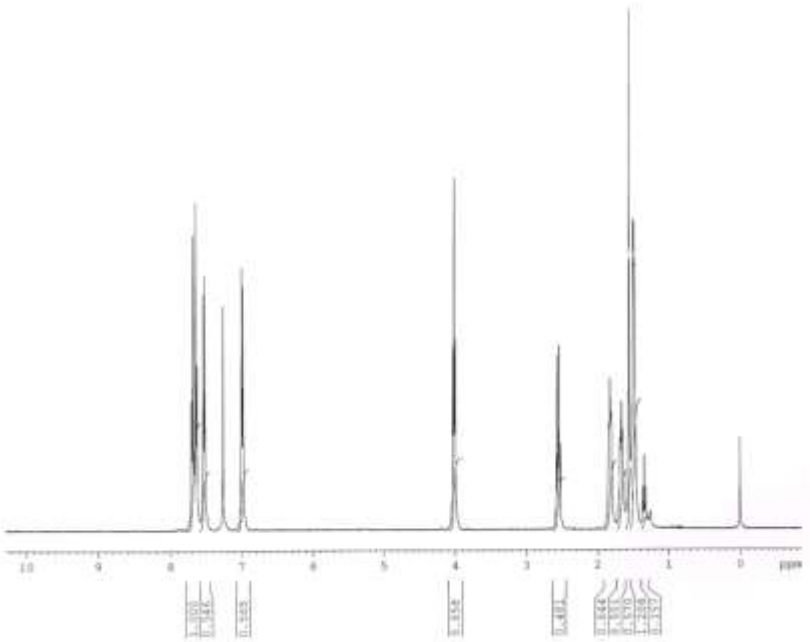

Figure 9. ^{1}H NMR spectrum of the compound **9b**.

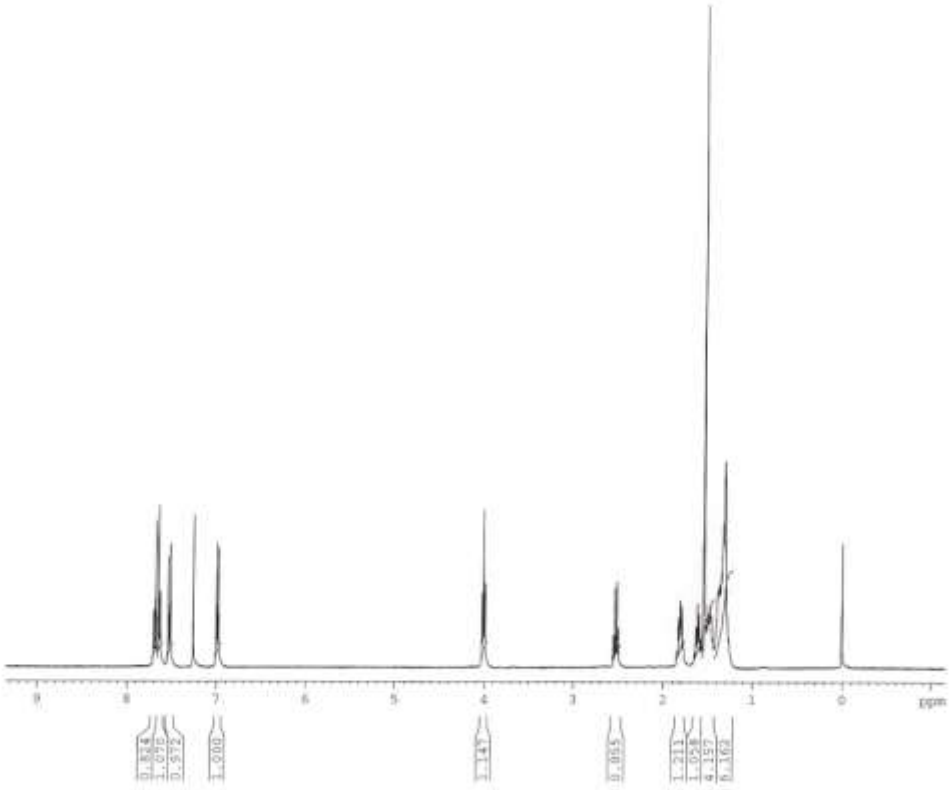

Figure 10. ^{1}H NMR spectrum of the compound **9f**.

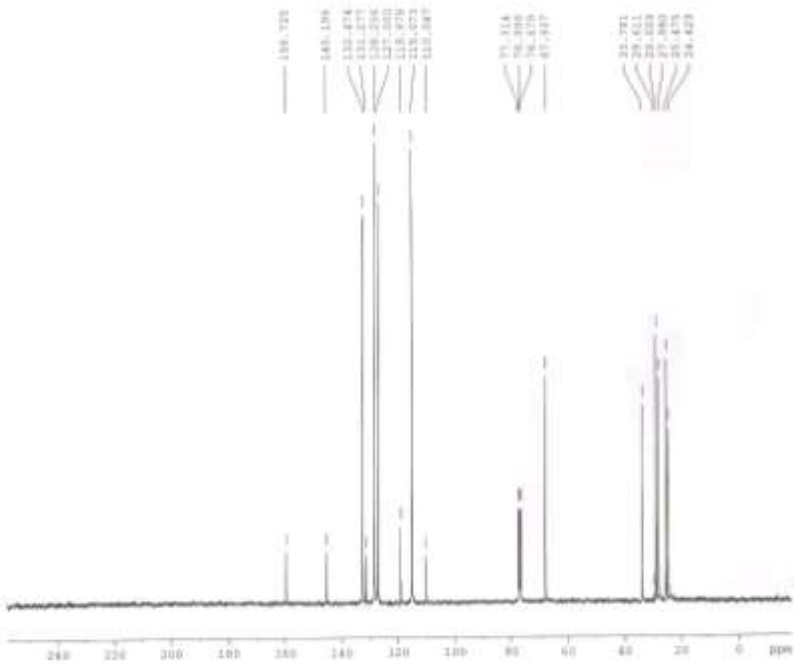

Figure 11. ^{13}C NMR spectrum of the compound **9b**.

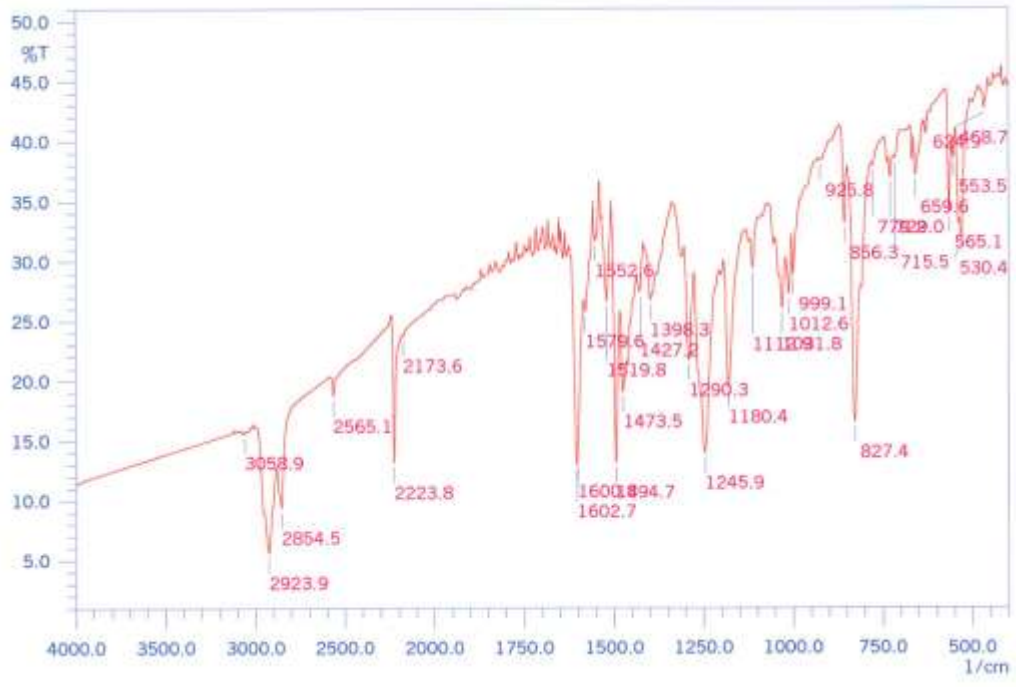

Figure 12. IR spectrum of the compound **9a**.

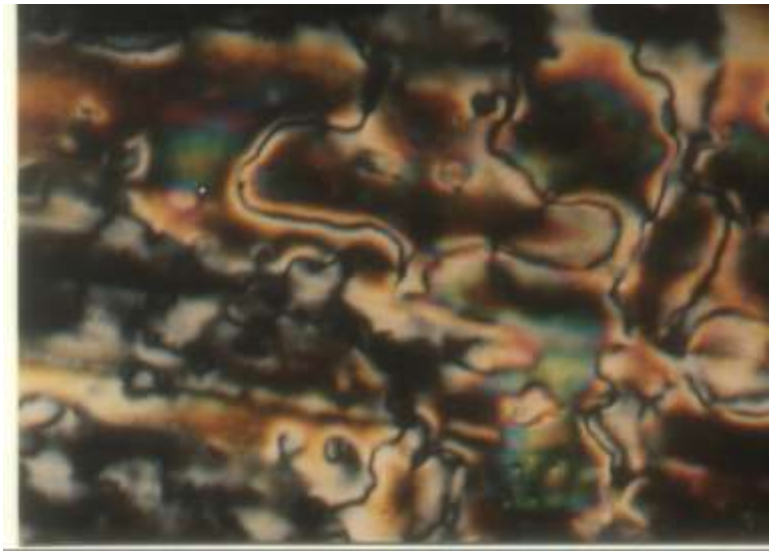

Figure 13. Optical texture of **9a** obtained on cooling from the isotropic liquid at 57 °C (Crossed polarizers, magnification X 200).

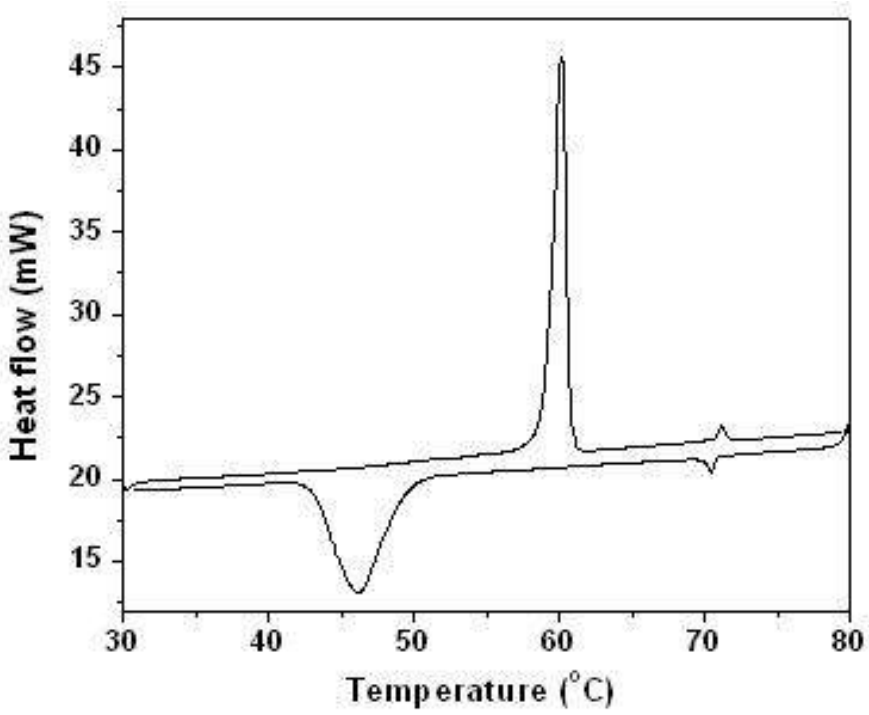

Figure 14. DSC traces of the compound **9c** on heating and cooling (5 °C/min).

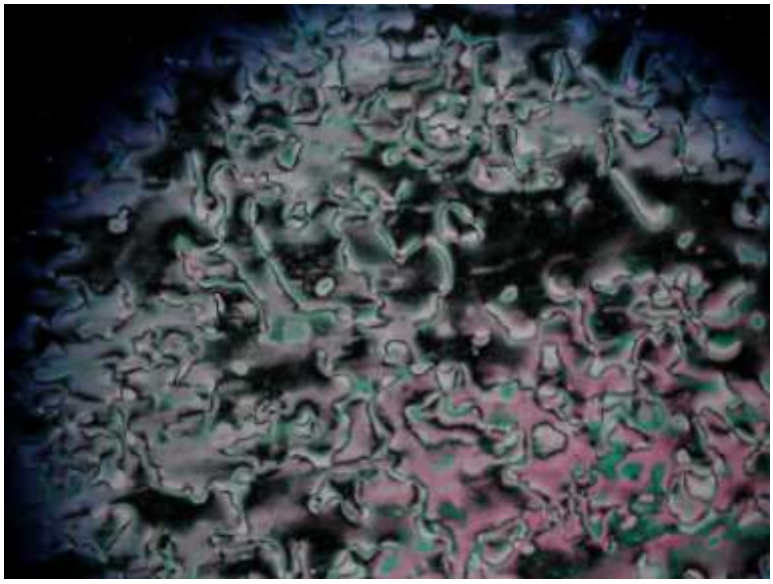

Figure 15. Optical texture of **9c** obtained on cooling from the isotropic liquid at 65 °C (Crossed polarizers, magnification X 200).

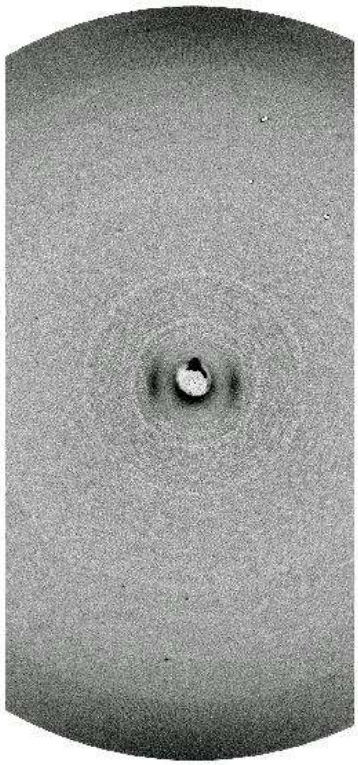

Figure 16. X-ray diffraction pattern obtained for compound **9f** at 60 °C.

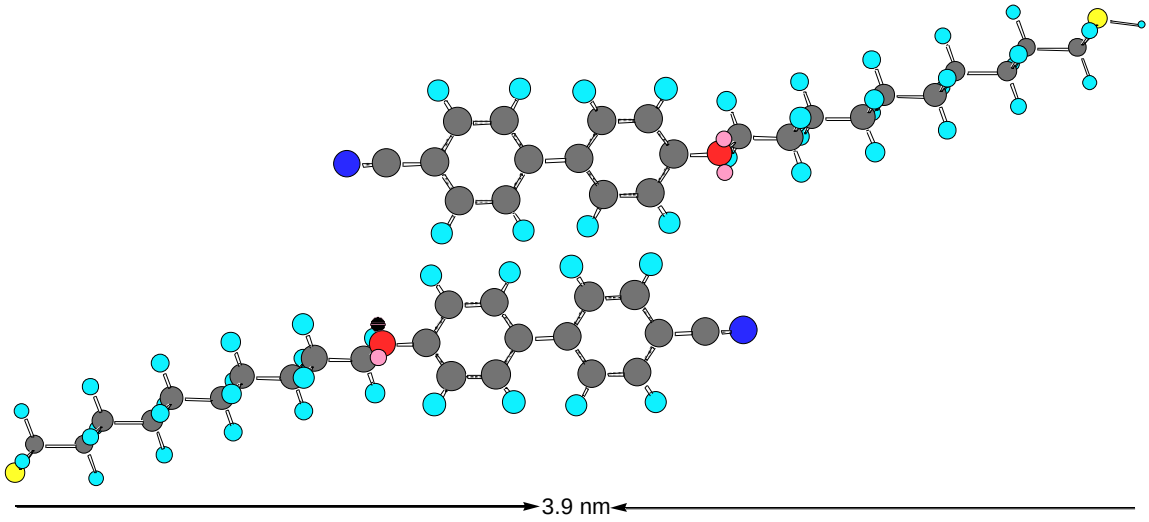

Figure 17. Sketch of the antiparallel arrangement of two biphenyls exhibited by **9f**.

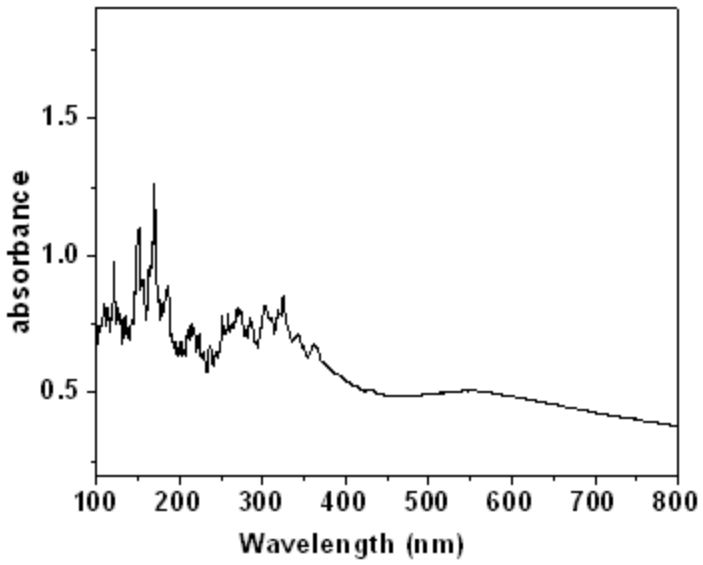

Figure 18. The UV-Vis spectrum of alkoxycyanobiphenyl covered GNPs.

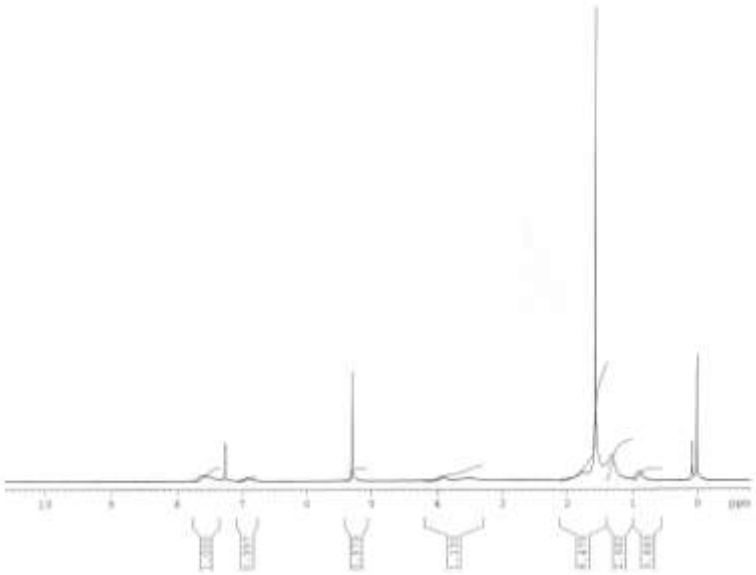

Figure 19. ^{1}H NMR spectrum of alkoxycyanobiphenyl-thiol covered GNPs.

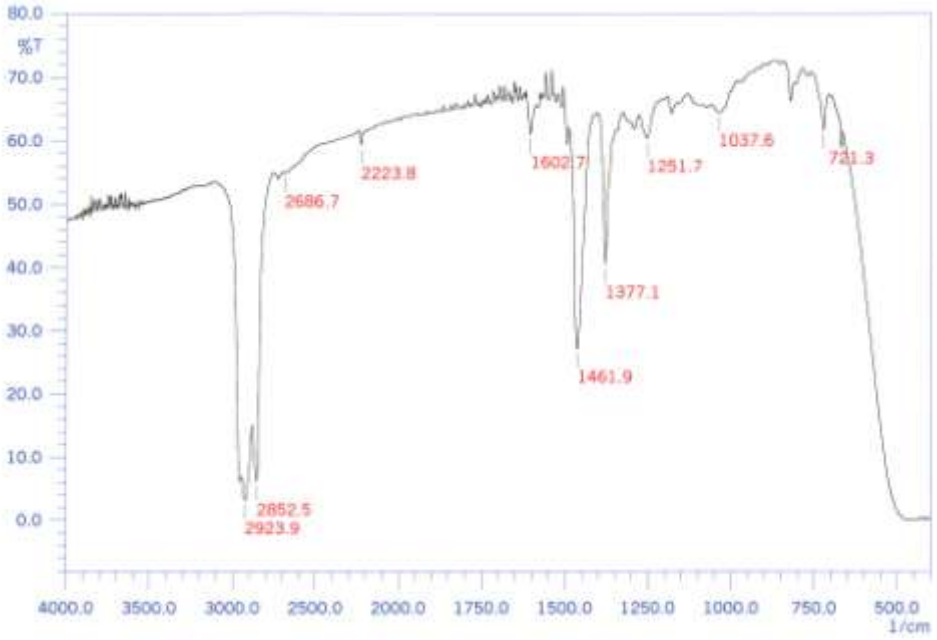

Figure 20. IR spectrum of alkoxycyanobiphenyl-thiol covered GNPs.

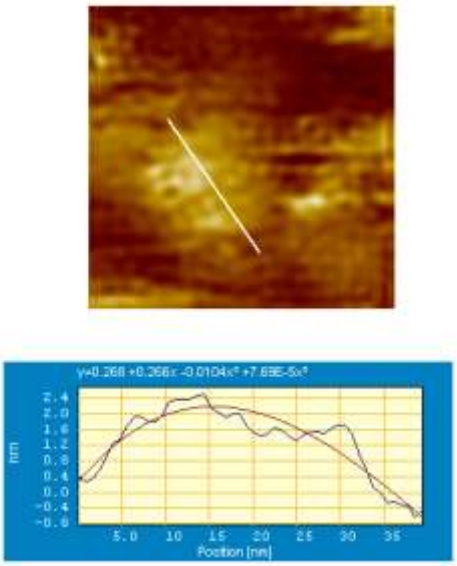

Figure 21. STM image of alkoxycyanobiphenyl-covered GNPs.

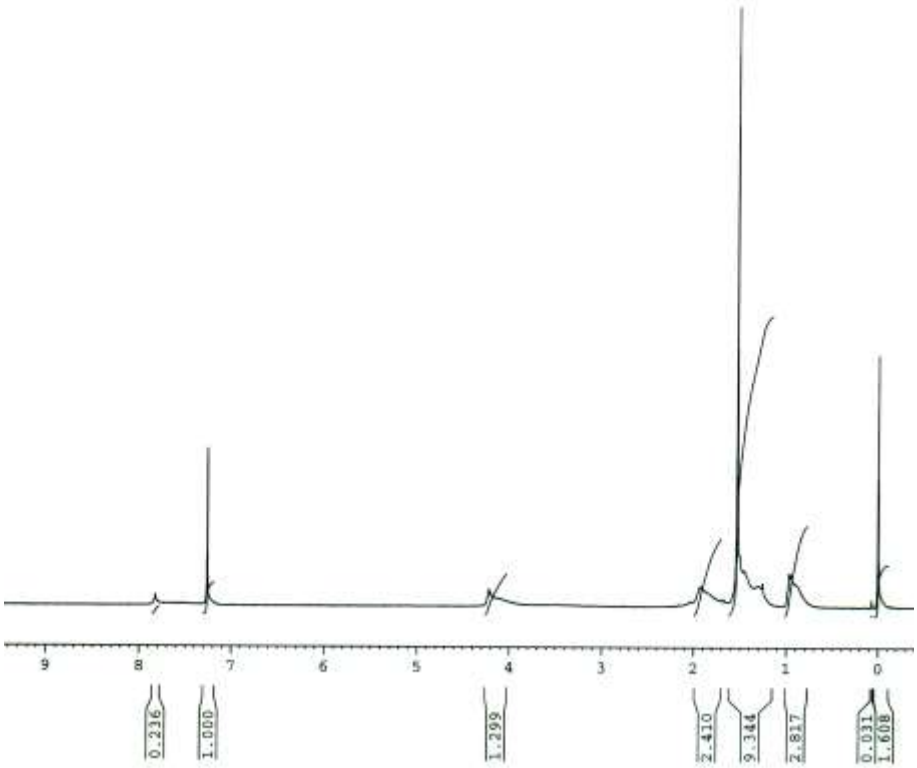

Figure 22. ^{1}H NMR spectrum of triphenylene-covered GNPs.

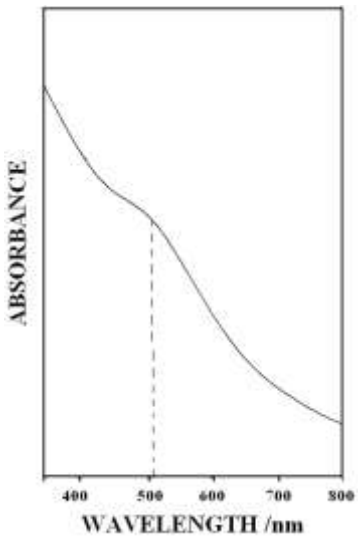

Figure 23. UV-Vis spectrum of triphenylene-covered gold nanoparticles. The characteristic surface plasmon absorption (SPR) at 505 nm can be clearly seen.

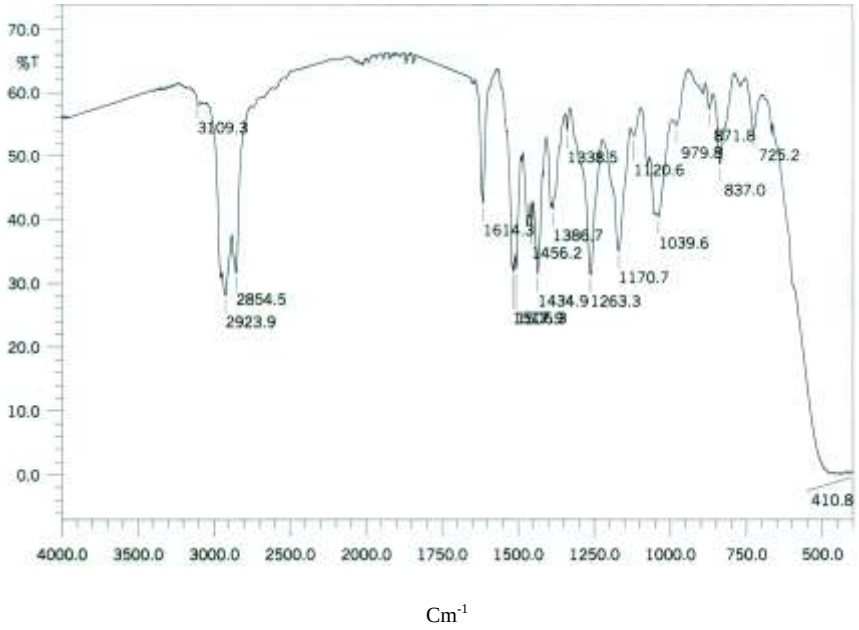

Figure 24. IR spectrum of triphenylene-covered gold nanoparticles.

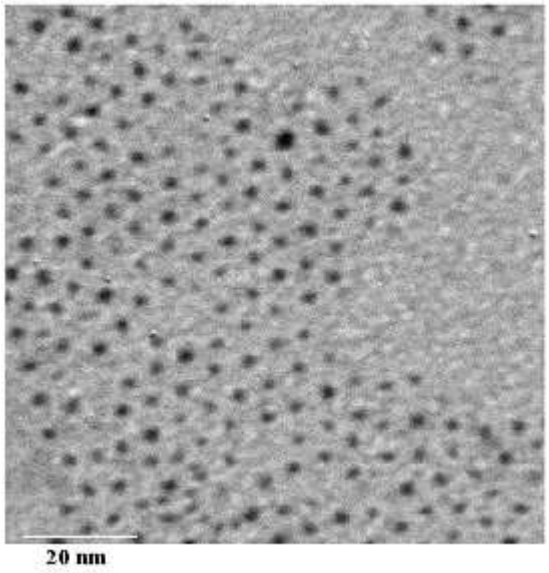

Figure 25. TEM image of triphenylene-capped gold nanoparticles

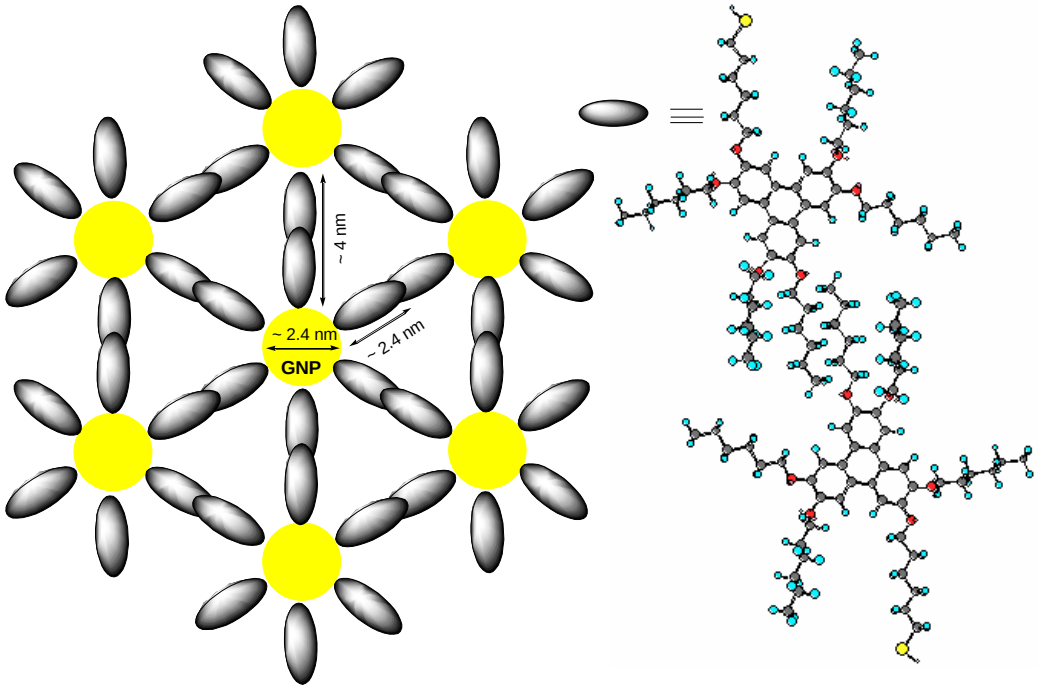

Figure 26. A cartoon for the hexagonal packing of triphenylene-capped gold nanoparticles as observed in TEM image.

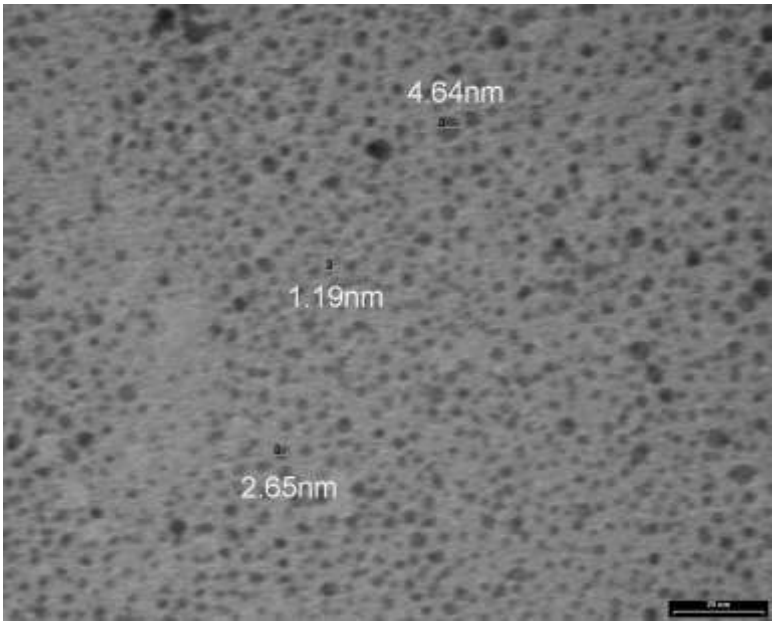

Figure 27. TEM image of mixed monolayers covered GNPs.

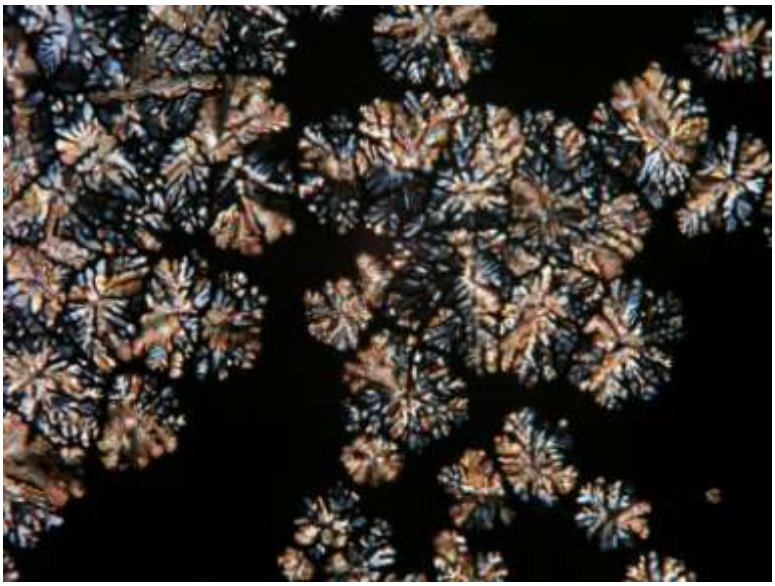

Figure 28. POM photograph of the columnar phase of **19c** at 85 °C (crossed polarizers, magnification X 100)

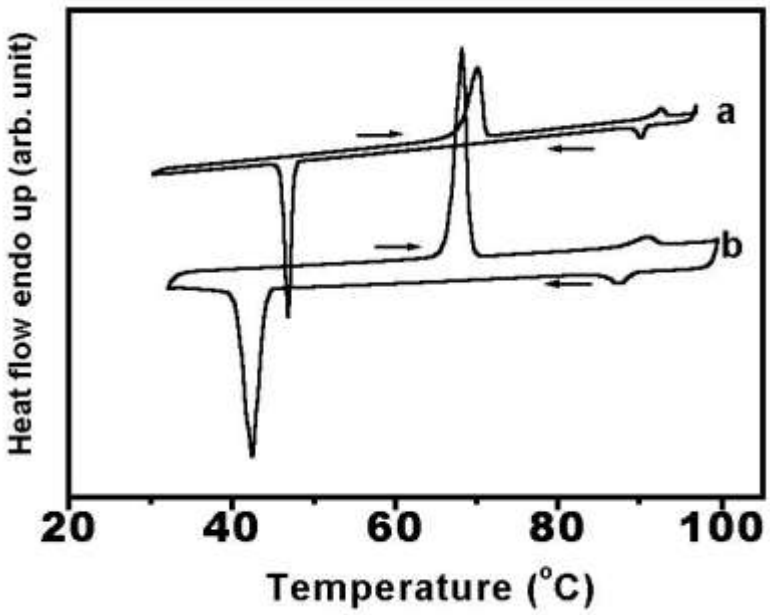

Figure 29. DSC traces for (a) H7TP and (b) for composite **19c** on heating and cooling (scan rate 5 °C min^{-1}).

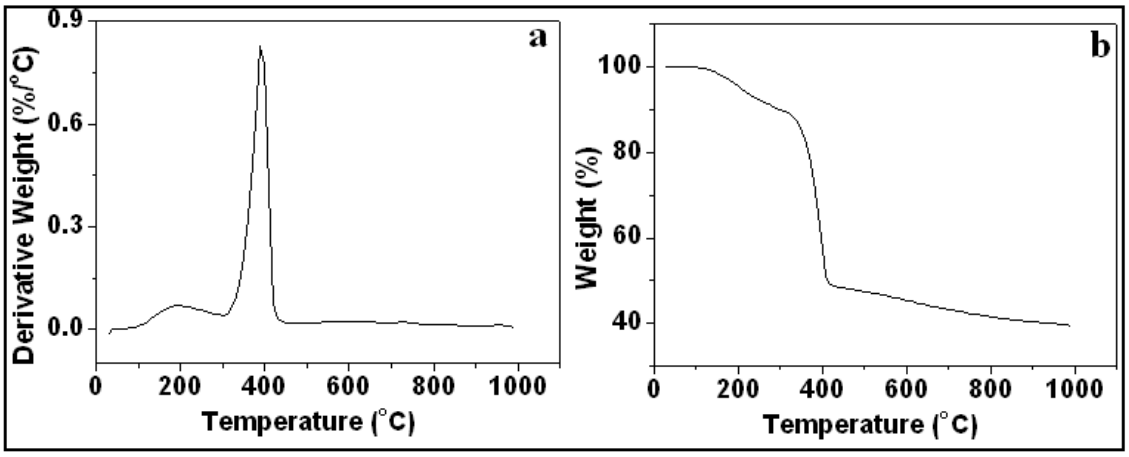

Figure 30. (a) The derivative weight (%) vs. temperature and (b) weight (%) vs. temperature (TGA) for triphenylene-covered gold nanoparticles

Figure 31. A schematic diagram illustrating arrangement of TP-GNPs in the inter domain spacing formed between the discotic columns.

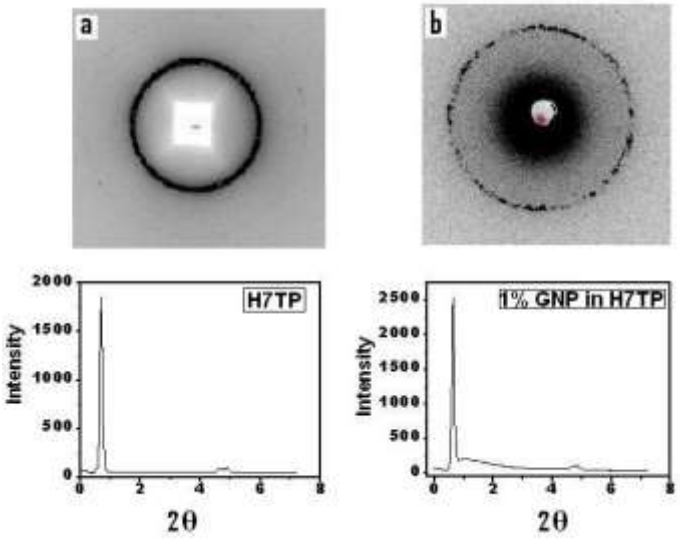

Figure 32. X-Ray diffraction pattern and the derived one-dimensional intensity *vs*. 2θ (deg.) profile for (a) H7TP and (b) for the composite **19b**.

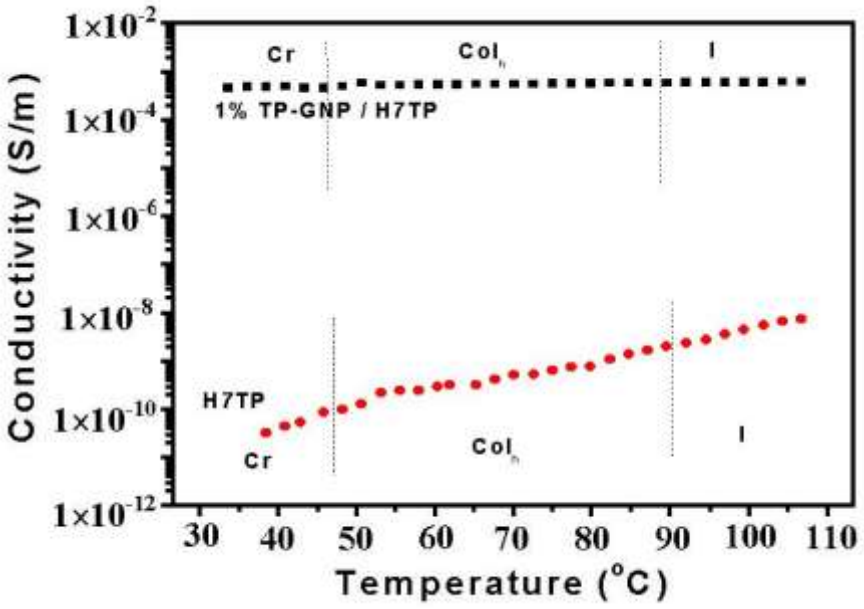

Figure 33. The variation of measured DC conductivity values as a function of temperature for 1% TP-GNPs mixed with H7TP and neat H7TP. The conductivities shown are obtained while cooling from isotropic phase. The vertical lines denote the phase transition temperatures obtained from the DSC studies.